



This is the accepted manuscript made available via CHORUS. The article has been published as:

## Dependence of

$\frac{n}{\gamma}$  equilibrium

process abundances on nuclear physics properties

Mengke Li and Bradley S. Meyer

Phys. Rev. C **106**, 035803 — Published 6 September 2022

DOI: [10.1103/PhysRevC.106.035803](https://doi.org/10.1103/PhysRevC.106.035803)

# Dependence of $(n, \gamma)$ - $(\gamma, n)$ Equilibrium r-Process Abundances on Nuclear Physics Properties

Mengke Li and Bradley S. Meyer

*Department of Physics and Astronomy,*

*Clemson University, Clemson, SC 29634-0978, USA*

(Dated: August 8, 2022)

## Abstract

In most r-process expansions, the dominant nuclear evolution occurs in an  $(n, \gamma)$ - $(\gamma, n)$  equilibrium in which nuclei rapidly exchange neutrons but change charge much more slowly by beta decay. Freezeout from this equilibrium shapes the final abundances but does not significantly alter the overall global abundance pattern; therefore, it is important to understand the details of  $(n, \gamma)$ - $(\gamma, n)$  equilibrium both because it is the main evolution phase that determines the final abundance pattern and because it is the starting point for the freeze out. Through use of a simple, but realistic, phenomenological nuclear physics model, we show that isotopic abundances versus neutron number in  $(n, \gamma)$ - $(\gamma, n)$  equilibrium are well approximated as Gaussians. Nuclear pairing causes isotopic abundances to alternate between two Gaussians, and shell effects cause the isotopic abundances to shift from one gaussian to another when the neutron number crosses a magic number. More complex neutron-separation energy curves versus mass number can be generated by adding a spike function to a linearly declining curve. In such a case, the equilibrium abundance curve jumps from one Gaussian to another for each added spike. Insights from our model can help shed light on how detailed theoretical or experimental nuclear data affect r-process nucleosynthesis during the  $(n, \gamma)$ - $(\gamma, n)$  equilibrium phase.

## I. INTRODUCTION

Many details of the origins of Nature's heaviest elements have long been understood [1]. In stars or stellar disruptions, seed nuclei can capture neutrons to increase their nuclear mass and beta decay to increase their nuclear charge. In a low neutron-density environment, neutron capture occurs more slowly than beta decay. This is the slow (s) process, and, owing to the slowness of the neutron captures, it only involves stable nuclei or nuclei near beta stability. In higher neutron-density environments, rapid capture of neutrons by seed nuclei leads to a population of neutron-rich isotopes that then increase their charge more slowly by beta decay. This is the rapid (r) process. As nuclei proceed through the sequence of neutron capture and beta decay in the r process, they eventually acquire a magic (closed neutron shell) number of neutrons. It is thermodynamically favorable for nuclei to retain this magic number of neutrons through the course of several beta decays, with each subsequent decay tending to take longer time than the previous one, before finally breaking away from this bottleneck number of neutrons and proceeding again more rapidly to higher charge. Since the r-process neutron captures are so rapid, the flow to higher charge is unimpeded by alpha decay. This is in contrast to the s-process flow, which terminates in the lead-bismuth region when nuclei are able to alpha decay faster than they capture neutrons. Only when r-process nuclei reach well into the actinide region do they become unstable to fission, a process that can occur much faster than neutron capture, and break into smaller fragments that begin their climb to higher mass and charge anew. This growth of nuclei by absorption of neutrons, mediated by beta decays to allow further neutron absorption, and interrupted by fission to create new seeds for further growth ceases when the supply of free neutrons disappears and nuclei decay to their ultimate stable daughters. Since a given nucleus spends most of its time during the r process with a magic number of neutrons, the final abundance distribution of the ensemble of nuclei undergoing this r (rapid) process shows peaks that arose from the high abundance of closed-shell progenitor species.

While this overall understanding of the r process is well in place, many research avenues remain open. Foremost among these is probably the pursuit of a detailed knowledge of the astrophysical site or sites that can provide the free neutron density and timescales appropriate for r-process nucleosynthesis. Sites involving ejecta from neutron stars have long been implicated, in particular, either from newly born neutron stars in a core-collapse

supernovae (e.g., [2–4]) or from disrupted neutron stars in merger events (e.g., [5–7]), but the exact setting or settings is not clear. In addition, the accretion disk forms in collapsars (the supernova-triggering collapse of rapidly rotating massive stars) is also expected to be the r-process elements production site [8].

Astronomical observations are providing crucial insights. The LIGO and Virgo observatories detected gravitational wave signal GW 170817 from the merger of two neutron stars [9]. Follow up observations of the electromagnetic signal counterparts to GW 170817 showed evidence of a kilonova [10], which is likely powered by the decay of r-process produced isotopes [11]. The significant implication is that neutron star mergers are indeed a site of r-process nucleosynthesis. This exciting result does not, however, rule out supernovae as another source of r-process isotopes. Models indicate that only certain rare supernovae, such as magnetorotational supernovae, can attain the conditions necessary to produce the heaviest r-process elements (e.g., [12]). Given the rarity of such events, direct detection is not likely forthcoming. On the other hand, observations of metal-poor stars provide key insights into early enrichment of the Galaxy by the r process (e.g., [13]), and comparison of detailed chemical evolution models to those observations can shed light on the relative contribution of supernovae and neutron-star mergers to r-process nucleosynthesis (e.g., [14]).

Another avenue of research into the r process that is of clear importance for the nuclear physics community is the question of how the properties of the nuclei involved in the nucleosynthesis influence the resulting r-process abundance pattern. As discussed above, the essential knowledge behind formation of the telltale r-process abundance peaks is understood. The precise shape and location of the peaks, however, depends on detailed knowledge of beta-decay rates along closed neutron shells. Experimental campaigns to measure these rates are crucial in providing this knowledge (e.g., [15]). Studies show, however, that it is not just decay rates along closed shells that are important for understanding the r-process abundance pattern—it is a full range of nuclear properties, including masses, cross sections, decay rates, and beta-delayed neutron emission probabilities that play a crucial role (e.g., [16, 17]). Many of these properties are being measured now or will be soon at facilities such as Radioactive Isotope Beam Factory (RIBF) in RIKEN or the Facility for Rare Isotope Beams (FRIB) at Michigan State University.

The nuclear properties governing r-process abundance patterns impose themselves during the nucleosynthesis; thus, the abundances result from nuclear reaction flows that arise from

the interplay of the nuclear properties and the thermodynamics of the expanding matter. This interplay therefore links the two questions discussed above: nuclear properties determine the reaction flows in the thermodynamic landscape largely determined by the particular expansion trajectory in a given astrophysical site. By studying how final r-process abundances depend on both the nuclear properties and thermodynamics, one may shed light on both the r-process site and the important nuclear properties for measurement or theoretical study.

One way of studying this interplay is to run a large suite of network calculations to explore the r-process abundances resulting from a range of thermodynamic trajectories for fixed nuclear physics (e.g., [18]) or from a range of nuclear properties for a set of chosen thermodynamic trajectories (e.g., [16, 19–22]). Such sensitivity studies provide valuable insight. They identify key nuclear parameters that govern final abundance distributions or particular trajectories that yield outcomes most similar to observed abundances. They also shed light on the range of abundance uncertainties that result from uncertainties in the nuclear or thermodynamic input. That knowledge can guide efforts to narrow the input uncertainties, either by nuclear experiment or more detailed computer modeling.

Another approach in studying the impact of the nuclear physics and thermodynamic trajectory on r-process abundances is to seek some general principles that can guide our understanding of how abundance patterns develop in the r process. With such knowledge, one can then predict the effect of variations in nuclear properties and/or trajectory thermodynamics on final abundances. Of course the original ideas regarding the development of the r-process peaks fall into this category. Such an approach also is important for understanding the origin of the rare-earth element peak in the r-process abundance pattern (e.g., [23, 24]).

Complicating this effort, however, is the fact that local variations in nuclear properties make the reaction flows that set abundances complex and difficult to follow in detail. Neighboring isotopes may have significantly varying rates for beta decay, neutron capture, or photodisintegration. This can make general flow patterns difficult to identify. Our approach then is to construct a simplified model of the nuclear properties important for the r process and use that model to gain insight into the details of the development of the r-process abundances. We then systematically add complexity to the nuclear model and study how those variations affect our understanding developed from the previous stage of complexity. At the final stage of complexity, our nuclear model matches realistic nuclear models well, so, by

our stepwise process, we are able to develop some general principles for understanding how nuclear properties and trajectory thermodynamics set r-process abundances.

In this paper, we apply our approach to the  $(n, \gamma)$ - $(\gamma, n)$  equilibrium phase of the r process. This is the phase in which the global abundance pattern is largely established in most r-process expansions. The first r-process network calculations assumed  $(n, \gamma)$ - $(\gamma, n)$  equilibrium [25] for computational feasibility.  $(n, \gamma)$ - $(\gamma, n)$  equilibrium, however, is not the phase that sets the final r-process abundances. That is the r-process freezeout in which a final flurry of reactions shuffle neutrons among the nuclei until all free neutrons have disappeared. Nevertheless,  $(n, \gamma)$ - $(\gamma, n)$ , or “classical”, r-process calculations have provided important insights into r-process flows and nuclear physics input (e.g., [26, 27]). Also good knowledge of  $(n, \gamma)$ - $(\gamma, n)$  equilibrium abundances provide a basis to study the freezeout in subsequent work since  $(n, \gamma)$ - $(\gamma, n)$  equilibrium is the starting point for the freezeout and is the goal of the system during freezeout, even if that goal is not reachable in the final moments of the nucleosynthesis.

We begin by discussing the  $(n, \gamma)$ - $(\gamma, n)$  equilibrium phase of the r process in the context of the full expansion of the matter from high temperature and density. The  $(n, \gamma)$ - $(\gamma, n)$  equilibrium isotopic abundances depend on the run of neutron-separation energy with mass number. We then demonstrate how that run depends on a mix of parameters in a simple nuclear mass model. That mix of parameters makes it difficult to cull the essential dependence of the equilibrium abundances on the neutron-separation energy as a function of mass number, so we develop our own nuclear model. To do so, we apply a finite calculus to turn power series expressions of neutron-separation and beta-decay energies into a nuclear mass model. We then use our nuclear mass model to understand  $(n, \gamma)$ - $(\gamma, n)$  equilibrium abundances in terms of our purely mathematical prescription. We then demonstrate how to use our model to understand equilibrium abundances from more realistic nuclear models. Finally, we show that our results can also be applied to proton-rich nucleosynthesis. Since  $(n, \gamma)$ - $(\gamma, n)$  equilibrium is the starting point for the r-process freezeout, our work sets the stage for understanding that final phase of the nucleosynthesis. In order to further illustrate the ideas in this paper, we have also prepared a number of Jupyter notebooks that allow the user to study  $(n, \gamma)$ - $(\gamma, n)$  equilibrium isotopic abundances with either our simple nuclear physics model or more realistic ones [28].

## II. $(n, \gamma) - (\gamma, n)$ EQUILIBRIUM

The nucleosynthesis of matter expanding from high temperature and density is well described as a “descent of the hierarchy of statistical equilibria” [29]. Each stage in the hierarchy is characterized by a set of rate-based constraints on the abundances which increase in number as time progresses in the expansion. The  $(n, \gamma) - (\gamma, n)$  equilibrium phase of r-process nucleosynthesis is one phase in the nucleosynthesis occurring in the expansion of neutron-rich matter in which isotopes are in equilibrium under exchange of neutrons due to the rapid neutron capture and disintegration reaction rates that prevail, but the isotope chains are not in equilibrium with each other due to the slowness of charged-particle and  $\beta^-$  decay rates that allow nuclei to flow from one element to another [30]. Much of the abundance pattern resulting from an r-process expansion is established in  $(n, \gamma) - (\gamma, n)$  equilibrium, so it is a crucial phase in the nucleosynthesis. That abundance pattern is shaped by final freezeout reactions after the  $(n, \gamma) - (\gamma, n)$  equilibrium breaks down.

To explore this evolution quantitatively, we follow the approach of comparing network abundances to constrained equilibria [29]. For a system at constant temperature and volume, or, equivalently, at constant mass density for a fixed number of nucleons, the change in the free energy per nucleon  $f$  is given by

$$df = \sum_i \mu_i dY_i \quad (1)$$

where  $\mu_i$  is the chemical potential  $i$  and  $Y_i$  is the abundance per nucleon of species  $i$ , respectively. Equilibrium abundances are then those abundances that give a free energy minimum such that  $df = 0$ . That minimum is subject to constraints. First, the general constraint is that the number of nucleons is fixed such that

$$\sum_Z \sum_A AY(Z, A) = 1 \quad (2)$$

where  $Y(Z, A)$  is the abundance per nucleon of the species with atomic number  $Z$  and mass number  $A$ . If the weak reaction timescales are long compared to other timescales in the problem, the electron-to-nucleon ratio  $Y_e$  may be taken to be fixed as well. For charge neutral matter, then, the constraint is

$$\sum_Z \sum_A ZY(Z, A) = Y_e \quad (3)$$

the condition  $df = 0$  with the constraints in Eqs. (2) and (3) results in the condition for nuclear statistical equilibrium (NSE)

$$\mu(Z, A) = Z\mu_p + (A - Z)\mu_n \quad (4)$$

where  $\mu_p$  and  $\mu_n$  are the chemical potentials of the free protons and neutrons, respectively.

Further constraints on equilibrium may be applied. If the sum of abundances of some cluster  $C$  of species changes slowly in time due to slow reaction rates, that abundance sum may be taken to be fixed such that

$$\sum_{i \in C} Y_i = Y_C \quad (5)$$

In this case, the quasi-equilibrium (QSE) condition results:

$$\mu(Z, A) = \tilde{\mu}(Z, A) + Z\mu_p + (A - Z)\mu_n \quad (6)$$

where  $\tilde{\mu}(Z, A)$  is a Lagrange multiplier (a chemical potential offset from NSE). The QSE condition is that all species  $i$  in the cluster  $C$  have the same chemical potential offset such that  $\tilde{\mu}(Z_i, A_i) = \mu_C$  for  $i \in C$ . The main QSE condition is that all heavy nuclei (nuclei with, say,  $Z > 2$ ) are in a single cluster. In this case, the nuclei in the cluster are able to exchange neutrons and protons as rapidly as required to maintain the QSE, but the total number of heavy nuclei is not changing in time because the three-body reactions assembling heavy nuclei from neutrons, protons, and alpha particles are slow [31].

In an expanding and cooling system, eventually new rates become too slow to maintain the QSE. New clusters appear, denoted  $C_j$  with index  $j$  distinguishing the different clusters. Each cluster has its own abundance constraint  $Y_{C_j}$ , analogous to Eq. 5, and its own chemical potential offset  $\tilde{\mu}_{C_j}$ . As the expansion continues, further clusters appear until final freezeout when there is a separate abundance constraint on each species.

r-process expansions typically proceed through such a history. The  $(n, \gamma) - (\gamma, n)$  equilibrium phase of the expansion is the stage when each isotope chain is an abundance cluster. Nuclei in the isotope chain exchange neutrons freely, but charged-particle reactions have frozen out. Nuclei increase charge by  $\beta^-$  decay only.

We explore this evolution with an r-process network calculation. The calculation used the NucNet Tools network code suite [32]. It began with an initial temperature  $T_9 = T/10^9 \text{ K} = 10$  and density  $\rho = 10^9 \text{ g/cc}$ . The initial electron fraction  $Y_e = 0.2$ , and the

matter expanded such that the density declined with time as  $\rho(t) = \rho(0) \exp(-t/\tau)$ , with  $\tau = 0.1$  s. The temperature behaved as  $\rho \propto T^3$ . The calculations ran for a total duration of  $10^6$  seconds.

Fig. 1 shows the chemical potential offset of a subset of species in the range from Cr ( $Z = 24$ ) to Ru ( $Z = 44$ ) in the network at time  $t = 0.243$  s into the expansion. At this moment, the temperature is  $T_9 = 4.44$  and the density is  $\rho = 8.78 \times 10^7$  g/cc. The color for each species shows the chemical potential offset relative to that for the most abundant species ( $^{79}\text{Cu}$ ) in the range of species in the figure at that moment in the expansion. To make a dimensionless quantity, the chemical potential offsets are also divided by  $kT$ , where  $k$  is Boltzmann's constant. The values of the scaled chemical potential offset for each species may be inferred from the color bar in Fig. 4. As is evident, all isotopes in the scope of the figure at this point in the expansion have a chemical potential offset near that of  $^{79}\text{Cu}$ . The high temperature means neutron-capture and charged-particle reaction rates are sufficiently large that all heavy isotopes are in equilibrium under exchange of neutrons and protons.

Fig. 2 shows the chemical potential offsets at  $t = 0.332$  s in the expansion. The temperature has dropped to  $T_9 = 3.30$  and the density has fallen to  $\rho = 3.60 \times 10^7$  g/cc. Differences in the chemical potential offsets are now evident. The most abundant species is  $^{84}\text{Zn}$ , with  $Z = 30$ . Isotopes with  $Z < 30$  have chemical potential offsets greater than that for  $^{84}\text{Zn}$ , which indicates that the abundance of those nuclei are in excess of the full QSE demands. In contrast, isotopes with  $Z > 30$  have chemical less than that for  $^{84}\text{Zn}$ . The spontaneous evolution of the system would favor a decrease in the free energy and therefore would favor a decrease in the abundance of  $Z < 30$  species and an increase in the abundance of  $Z > 30$  isotopes. At this point in the expansion, however, the charged-particle reactions that would effect this change are too slow to keep up with the equilibrium demands. Within an isotope chain, however, chemical potential offsets are uniform, which means that neutron capture and disintegration reactions are sufficiently fast to maintain the equilibrium under exchange of neutrons.

Fig. 3 shows the chemical potential offsets at  $t = 0.432$  s. The temperature has dropped further to  $T_9 = 2.369$  and the density is  $\rho = 1.33 \times 10^7$  g/cc. By this point, isotope chains, while still in equilibrium under exchange of neutrons, are now largely out of equilibrium with each other due to the slowness of the charged-particle reactions. The network is entering the  $(n, \gamma) - (\gamma, n)$  equilibrium phase of the expansion. From this point on, nuclei increase

their charge only by  $\beta^-$  decays. The double-outlined circles in the figure give the abundance maximum for each isotope chain (other than the one with the overall maximum); therefore, the locus of these circles (plus the triple-outlined octagon) is the “r-process path” at this moment, and the path shows the characteristic kinks along the closed shells at neutron numbers  $N = 50$  and  $N = 82$  due to the strong neutron binding at those magic numbers.

The  $(n, \gamma) - (\gamma, n)$  equilibrium phase is crucial for the r process expansion because it is here that the global abundances are set. Fig. 5 shows the network abundances versus mass number  $A$  at the last moment when the  $(n, \gamma) - (\gamma, n)$  equilibrium holds and at the end of the calculation. The last moment of the equilibrium is when the isotopic equilibrium abundances first start to deviate from the network isotopic abundances, or, equivalently, when the neutron-capture reaction flows no longer balance the photodissociation flows. We recognize that there is not a single moment when all isotope chains fall out of  $(n, \gamma) - (\gamma, n)$  equilibrium. Nevertheless, the spread in times when the different chains fall out of equilibrium is quite narrow relative to the duration of the nucleosynthesis; thus, the last equilibrium abundances in Fig. 5 are indeed a good representation of the network abundances at the end of  $(n, \gamma) - (\gamma, n)$  equilibrium.

The figure shows the dramatic smoothing (that is, the reduction of the variation of abundances versus mass number) that occurs during the freezeout from the  $(n, \gamma) - (\gamma, n)$  equilibrium, but it also shows that smoothing is largely just a reshaping of the global abundance pattern that was already set during the  $(n, \gamma) - (\gamma, n)$  equilibrium.

Because species with the same atomic number  $Z$  have the same chemical potential offset in  $(n, \gamma) - (\gamma, n)$  equilibrium, it is clear that

$$\mu(Z, A) - \mu(Z, A - 1) = \mu_n \tag{7}$$

which is the well-known  $(n, \gamma) - (\gamma, n)$  equilibrium condition [1]. In the form  $\mu(Z, A) = \mu(Z, A - 1) + \mu_n$ , it expresses the equilibrium as the condition that the neutron capture reaction on  $(Z, A - 1)$ , which adds a species  $(Z, A)$  with free energy cost  $\mu(Z, A)$ , is balanced by the disintegration reaction on  $(Z, A)$ , which adds a species  $(Z, A - 1)$  and a neutron  $n$  with free energy cost  $\mu(Z, A - 1) + \mu_n$ .

Another interpretation of Eq. (7) is possible.  $\mu_n$  is the chemical potential of the free neutrons, that is, the neutrons outside of nuclei; thus, we can label  $\mu_n = \mu_n^{(out)}$ . We imagine transferring some of those neutrons to species  $(Z, A - 1)$ . In this case,

$dY(Z, A) = -dY(Z, A - 1) = -dY_n$ , and the free energy change (Eq. (1)) is

$$df = (\mu(Z, A) - \mu(Z, A - 1))(-dY_n) - \mu_n^{(out)}dY_n \quad (8)$$

We now note that  $-dY_n$  is the increase in the number of neutrons per nucleon contained in species  $(Z, A)$ ; thus, we infer that the chemical potential of neutrons inside nucleus  $(Z, A)$  is

$$\mu_n^{(in)}(Z, A) = \mu(Z, A) - \mu(Z, A - 1) \quad (9)$$

in which case,  $(n, \gamma) - (\gamma, n)$  equilibrium is the condition that the chemical potential of neutrons inside each nuclear species is equal to the chemical potential of neutrons outside the nuclei:  $\mu_n^{(in)}(Z, A) = \mu_n^{(out)}$ .

The chemical potential of species  $i$  may be written in terms of the rest mass  $m_i$  as  $\mu_i = m_i c^2 + \mu'_i$ , in which case Eq. (7) may be written

$$\mu'(Z, A) - \mu'(Z, A - 1) = \mu'_n + S_n(Z, A) \quad (10)$$

where  $S_n(Z, A)$  is the neutron-separation energy

$$S_n(Z, A) = m(Z, A - 1)c^2 + m_n c^2 - m(Z, A)c^2 \quad (11)$$

Under the largely valid assumption that all species undergoing r-process nucleosynthesis are non-interacting and non-relativistic, the chemical potential of species  $(Z, A)$  is given by

$$\mu'(Z, A) = kT \ln \left[ \frac{\rho N_A Y(Z, A)}{G(Z, A)} \left( \frac{2\pi\hbar}{m(Z, A)kT} \right)^{\frac{3}{2}} \right] \quad (12)$$

In this equation,  $N_A$  is Avogadro's number and  $G(Z, A)$  is the nuclear partition function. From these equations, we can thus write

$$\frac{Y(Z, A)}{Y(Z, A - 1)} = \frac{G(Z, A)}{G(Z, A - 1)} \left[ \frac{m(Z, A)}{m(Z, A - 1)} \right]^{3/2} \exp \left\{ \frac{1}{kT} [\mu'_n + S_n(Z, A)] \right\} \quad (13)$$

This equation shows the relative abundances of neighboring species in an isotopic chain in  $(n, \gamma) - (\gamma, n)$  equilibrium. Products of such ratios will give the abundance of species  $(Z, A)$  relative to the species  $(Z, A_0)$  at the beginning of the isotope chain:

$$\begin{aligned} \frac{Y(Z, A)}{Y(Z, A_0)} &= \frac{Y(Z, A)}{Y(Z, A - 1)} \times \frac{Y(Z, A - 1)}{Y(Z, A - 2)} \times \dots \times \frac{Y(Z, A_0 + 1)}{Y(Z, A_0)} \\ &= \frac{G(Z, A)}{G(Z, A_0)} \left[ \frac{m(Z, A)}{m(Z, A_0)} \right]^{3/2} \exp \left\{ \frac{1}{kT} \left[ (A - A_0) \mu'_n + \sum_{A'=A_0+1}^A S_n(Z, A') \right] \right\} \quad (14) \end{aligned}$$

The abundances  $Y(Z, A)$  in Eq. (14) are scaled to the abundance at the beginning of the isotopic chain. They can be normalized as appropriate, for example, to give the total isotopic abundance in a corresponding network calculation or to give the maximum abundance in the chain a value of unity. In what follows, we thus refer to Eq. (14) as the  $(n, \gamma) - (\gamma, n)$  equilibrium isotopic abundance distribution for element  $Z$ .

### III. NEUTRON-SEPARATION ENERGY DEPENDENCE ON MASS NUMBER

Eq. (14) shows that the abundances in an isotope chain in  $(n, \gamma) - (\gamma, n)$  equilibrium depend on the variation of the neutron-separation energy with mass number  $A$ . To get a sense of that variation, we consider a simple liquid-drop model for the nucleus [33]. In this semi-empirical model, the rest mass energy for a nuclear species  $(Z, A)$  is given by

$$m(Z, A)c^2 = Zm_p c^2 + (A - Z)m_n c^2 - a_V A + a_S A^{2/3} + a_C \frac{Z^2}{A^{1/3}} + a_A \frac{(A - 2Z)^2}{A} \quad (15)$$

where the last four terms are the volume term, surface term, Coulomb term, and asymmetry term, respectively. With this formula, the neutron-separation energy can be written as

$$S_n(Z, A) = a_V - a_A - a_S [A^{2/3} - (A - 1)^{2/3}] - a_C Z^2 [A^{-1/3} - (A - 1)^{-1/3}] - 4a_A Z^2 [A^{-1} - (A - 1)^{-1}] \quad (16)$$

In order to find the run of neutron-separation energy with mass number, we simultaneously expand  $S_n$  in a Taylor and power series about  $A_0$ . Thus, we write

$$S_n(Z, A) = \sum_{k=0}^{\infty} \frac{1}{k!} \left( \frac{\partial^k S_n}{\partial A^k} \right)_{A_0} (A - A_0)^k \quad (17)$$

and

$$S_n(Z, A) = \sum_{k=0}^{\infty} S_k (A_0 - A)^k \quad (18)$$

The power series coefficients  $S_k$  in Eq. (18) are then given by

$$S_k = (-1)^k \frac{1}{k!} \left( \frac{\partial^k S_n}{\partial A^k} \right)_{A_0} \quad (19)$$

By computing the derivative of Eq. (16) and making the largely valid assumption that  $A_0 \gg 1$ , we find

$$S_k = \frac{C_s (a_S A_0^{2/3}) + C_c \frac{a_C Z^2}{A_0^{1/3}} + C_a \frac{4a_A Z^2}{A_0}}{A_0^{k+1}} + C_0 \quad (20)$$

where

$$\begin{aligned}
C_s &= \frac{-2(3k-2)!!!}{3^{k+1}k!} \\
C_c &= \frac{(3k+1)!!!}{3^{k+1}k!} \\
C_a &= k+1
\end{aligned}
\tag{21}$$

with the triple-factorial defined as  $x!!! = x(x-3)(x-6)\dots$  with the understanding that any term in the product less than or equal to zero should be set to one. For  $k=0$ ,  $C_0 = a_V - a_A$ , otherwise  $C_0 = 0$ .

From Eq. (20), we may notice that the power-series coefficients are a complex mix of terms in the liquid-drop model. This is even more true for more complex nuclear physics models that include other macroscopic or microscopic terms. Such complexities make it difficult to disentangle the effects of variations of nuclear mass model properties on  $(n, \gamma) - (\gamma, n)$  equilibrium abundances. Our approach instead will be to assume a power-series form for the neutron-separation energy, as in Eq. (18), and study the dependence of the abundances on individual coefficients. We will then add microscopic effects due to neutron pairing and shell phenomena. With a good understanding of the dependence of abundances on the power-series coefficients (and simple shell and pairing parameterizations), one may then compare particular nuclear mass models to our parameterizations to infer how isotopic abundances will depend on the details of those models.

From Eq. (20), we may also notice that  $\frac{S_{k+1}}{S_k} \sim \mathcal{O}(\frac{1}{A_0})$ . This means that, as long as  $A - A_0 \lesssim A_0$ , the power-series expansion of  $S_n$  will be dominated by the lowest-order terms. We will find it sufficient to restrict our considerations to  $k \leq 2$ .

#### IV. FINITE CALCULUS

The isotopes of nature are distinguished by integer numbers of nucleons, and the properties of these isotopes are functions of these nucleon numbers or differences between them. For this reason, it is convenient for our purpose of studying the dependence of isotopic abundances on power-series expansions of nuclear properties to use a “discrete” or “finite” calculus to derive and characterize these quantities.

## A. Finite Differentiation

Finite differences (our “finite derivatives”) were introduced by Taylor in 1715 [34] and have played an important role in the development of calculus and computational mathematics. This section introduces our notation.

In continuous calculus, the partial derivative of a multivariate function  $f(x, y)$  is defined as

$$\left(\frac{\partial f(x, y)}{\partial x}\right)_y = \lim_{\Delta x \rightarrow 0} \frac{f(x + \Delta x, y) - f(x, y)}{\Delta x} \quad (22)$$

To denote our finite derivatives, we proceed analogously. The step  $\Delta x$  away from  $x$  is constrained to have unit value. Consider a function  $F(x, y)$ , where  $x$  is the integer variable of interest and  $y$  is an integer variable or set of variables other than  $x$ . Now  $\Delta x = 1$  can be taken in one of two directions. We denote the *backward* derivative of  $F$  as

$$\left[\frac{\partial F(x, y)}{\partial x}\right]_y^- \equiv F(x, y) - F(x - 1, y) \quad (23)$$

Similarly, we denote the *forward* derivative of  $F$  as

$$\left[\frac{\partial F(x, y)}{\partial x}\right]_y^+ \equiv F(x + 1, y) - F(x, y) \quad (24)$$

In either case, the subscript  $y$  indicates that the variable (or set of variables)  $y$  is held constant.

There are cases where it is useful to consider quantities such as  $F(x, y) - F(x - 2, y)$ . It is a simple matter to show that

$$F(x, y) - F(x - 2, y) = \left[\frac{\partial F(x, y)}{\partial x}\right]_y^- + \left[\frac{\partial F(x - 1, y)}{\partial x}\right]_y^- \quad (25)$$

## B. Finite Integration

In continuous calculus, the integral of a function may be defined in terms of a Riemann sum. Suppose  $[a, b]$  is a closed interval of real numbers and  $f(x, y)$  is a function that maps real numbers  $x \in [a, b]$  to real numbers. The variable  $y$  is a real number or set of real numbers that remains fixed during the mapping. We let

$$P = \{[x_0, x_1], [x_1, x_2], \dots, [x_{n-1}, x_n]\} \quad (26)$$

be a partition of the real numbers over  $[a, b]$ , with

$$a = x_0 < x_1 < x_2 < \dots < x_n = b \quad (27)$$

We may define our integral as

$$\int_a^b f(x, y) dx = \lim_{n \rightarrow \infty} \sum_{i=1}^n f(x_i^*, y) \Delta x_i \quad (28)$$

where  $\Delta x_i = x_i - x_{i-1}$  and  $x_i^* \in [x_{i-1}, x_i]$ .

We proceed analogously to define our finite integrals. We consider two integers  $a$  and  $b$ , with  $a < b$ , and the closed interval of integers  $[a, b]$ . We consider a function  $F(x, y)$  that maps integer  $x \in [a, b]$  to numbers. We let

$$P = \{[x_0, x_1], [a + 1, x_2], \dots, [x_{n-1}, x_n]\} \quad (29)$$

be a partition of the integers over  $[a, b]$ , with

$$a = x_0 < x_1 = a + 1 < x_2 = a + 2 < \dots < x_{n-1} = b - 1 < x_n = b \quad (30)$$

Since the variable  $x$  in  $F(x, y)$  is now integer, we have an ambiguity in defining  $x_i^*$ : it must either be  $x_{i-1}$  or  $x_i$ . In the former case, our finite integral becomes

$$\left[ \int_a^b F(x, y) dx \right]^- = \sum_{i=0}^{n-1} F(x_i, y) = \sum_{x=a}^{b-1} F(x, y) \quad (31)$$

In the latter case, our finite integral becomes

$$\left[ \int_a^b F(x, y) dx \right]^+ = \sum_{i=1}^n F(x_i, y) = \sum_{x=a+1}^b F(x, y) \quad (32)$$

The limits on the sums show that we are to understand both integrals to be zero in the case  $a = b$

The superscripts in finite derivatives and finite integrals so defined are such that integrals can properly be considered the antiderivatives of the finite derivatives of *opposite* superscripts, where the  $\pm$  of a derivative in a sense undoes the  $\mp$  of an integral, and vice versa. Explicitly, this means,

$$\left[ \frac{\partial}{\partial x} \left[ \int_{x_0}^x F(x', y) dx' \right]^- \right]^+ = F(x, y) \quad (33)$$

and

$$\left[ \frac{\partial}{\partial x} \left[ \int_{x_0}^x F(x', y) dx' \right]^+ \right]^- = F(x, y) \quad (34)$$

### C. Application to Polynomials

In most cases, we will deal with polynomial integer functions. This means we consider functions built up of terms like  $F(x, y) = Cx^p y^q$ , where  $C$  is a constant and  $p$  and  $q$  are integers. In general, if we focus on  $x$ , the  $Cy^q$  term will be a simple multiplicative factor on the resulting derivative or integral. In such a case, we may compute

$$\left[ \frac{\partial}{\partial x} (x^p) \right]_y^- = x^p - (x-1)^p = \sum_{k=0}^{p-1} \binom{p}{k} x^k (-1)^{p-k+1} \quad (35)$$

Here  $\binom{p}{k}$  is the usual binomial coefficient. Similarly,

$$\left[ \frac{\partial}{\partial x} (x^p) \right]_y^+ = (x+1)^p - x^p = \sum_{k=0}^{p-1} \binom{p}{k} x^k \quad (36)$$

For either derivative, the leading term is  $px^{p-1}$ , as expected from continuous calculus, but there are other terms due to our discrete treatment. For the special case  $p = 0$ , and in the case of any constant with respect to the variable of differentiation, the finite derivatives work out to  $x^0 - (x-1)^0 = (x+1)^0 - x^0 = 1 - 1 = 0$ . Table I shows both kinds of derivatives for the first few values of  $p$ .

| p | $\left[ \frac{\partial}{\partial x} (x^p) \right]_y^+$ | $\left[ \frac{\partial}{\partial x} (x^p) \right]_y^-$ |
|---|--|--|
| 0 | 0  | 0  |
| 1 | 1  | 1  |
| 2 | $2x + 1$   | $2x - 1$   |
| 3 | $3x^2 + 3x + 1$  | $3x^2 - 3x + 1$  |

TABLE I: Finite derivatives of  $x^p$  for  $p = 0, 1, 2, 3$ .

For integrals, we find

$$\left[ \int_{x_0}^x x'^p dx' \right]^- = \sum_{x'=x_0}^{x-1} x'^p = \sum_{x'=0}^{x-1} x'^p - \sum_{x'=0}^{x_0-1} x'^p \quad (37)$$

This may be written

$$\left[ \int_{x_0}^x x'^p dx' \right]^- = \frac{1}{p+1} [B_{p+1}(x) - B_{p+1}(x_0)] \quad (38)$$

where  $B_{p+1}(x)$  is the Bernoulli polynomial of order  $p + 1$ . The explicit formula for the Bernoulli polynomial of order  $n$  is

$$B_n(x) = \sum_{k=0}^n \binom{n}{k} B_{n-k} x^k \quad (39)$$

where  $B_{n-k}$  is the Bernoulli number of order  $n-k$ . The Bernoulli number  $B_n$  is the Bernoulli polynomial  $B_n(x)$  evaluated at  $x = 0$ . Table II shows the first few Bernoulli polynomials.

| p | $B_p(x)$                              |
|---|---------------------------------------|
| 0 | 1                                     |
| 1 | $x - \frac{1}{2}$                     |
| 2 | $x^2 - x + \frac{1}{6}$               |
| 3 | $x^3 - \frac{3}{2}x^2 + \frac{1}{2}x$ |

TABLE II: The first four Bernoulli polynomials.

For  $B_p(x)$ , the highest-power term of  $x$  is  $x^p$ ; thus, the leading term in  $x$  in Eq. (38) is  $\frac{1}{p+1} [x^{p+1} - x_0^{p+1}]$ , as expected from continuous calculus, although the full finite integral is a sum of many terms.

We similarly find

$$\left[ \int_{x_0}^x x'^p dx' \right]^+ = \frac{1}{p+1} [B_{p+1}(x+1) - B_{p+1}(x_0+1)] \quad (40)$$

The leading term for this integral is  $\frac{1}{p+1} [x^{p+1} - x_0^{p+1}]$ , which again is as expected. Table III shows the integrals for the first few values of  $p$ .

It is evident, but also explicitly confirmed in Appendix A, that a change of variable  $u = x' - x_0$  leads to

$$\left[ \int_{x_0}^x (x' - x_0)^p dx' \right]^+ = \left[ \int_0^{x-x_0} u^p du \right]^+ = \frac{1}{p+1} [B_{p+1}(x-x_0+1) - B_{p+1}(1)] \quad (41)$$

One similarly finds

$$\left[ \int_{x_0}^x (x' - x_0)^p dx' \right]^- = \frac{1}{p+1} [B_{p+1}(x-x_0) - B_{p+1}] \quad (42)$$

From the relation between Bernoulli polynomials  $B_n(x)$  that

$$B_n(x+1) - B_n(x) = nx^{n-1} \quad (43)$$

| p | $\left[ \int_{x_0}^x x'^p dx' \right]^+$                                       | $\left[ \int_{x_0}^x x'^p dx' \right]^-$                                       |
|---|--|--|
| 0 | $x - x_0$  | $x - x_0$  |
| 1 | $\frac{1}{2}[(x^2 - x_0^2) + (x - x_0)]$                                       | $\frac{1}{2}[(x^2 - x_0^2) - (x - x_0)]$                                       |
| 2 | $\frac{1}{3}[(x^3 - x_0^3) + \frac{3}{2}(x^2 - x_0^2) + \frac{1}{2}(x - x_0)]$ | $\frac{1}{3}[(x^3 - x_0^3) - \frac{3}{2}(x^2 - x_0^2) + \frac{1}{2}(x - x_0)]$ |
| 3 | $\frac{1}{4}[(x^4 - x_0^4) + 2(x^3 - x_0^3) + (x^2 - x_0^2)]$                  | $\frac{1}{4}[(x^4 - x_0^4) - 2(x^3 - x_0^3) + (x^2 - x_0^2)]$                  |

TABLE III: Finite integrals of  $x^p$  for  $p = 0, 1, 2, 3$ .

it is clear that the inverse relations in Eqs. (33) and (34) between finite derivatives and integrals hold for these polynomial forms.

For completeness, we note some relations for functions with  $F(x) = x^{-p}$ , where  $p$  is an integer and  $p > 0$ , in Appendix B.

## V. NUCLEAR PHYSICS

Isotopes are distinguished by the atomic number  $Z$  and mass number  $A$ . The rest mass of an isotope  $(Z, A)$  is  $M(Z, A)c^2$ , with  $c$  the speed of light. The rest mass of species  $(Z, A)$  can be quantified conveniently in terms of the mass excess  $\Delta(Z, A)$  such that

$$M(Z, A)c^2 = AM_u c^2 + \Delta(Z, A) \quad (44)$$

where  $M_u$  is the atomic mass unit (masses are typically given in terms of atomic masses, which include the electrons). The binding energy  $B(Z, A)$  of a species, which is the excess of the masses of the constituent nucleons over the mass of the species is then

$$B(Z, A) = Z\Delta(1, 1) + (A - Z)\Delta_n - \Delta(Z, A) \quad (45)$$

where  $\Delta_n$  is the mass excess of the free neutron.

The neutron-separation energy  $S_n(Z, A)$  is the minimum energy required to remove a neutron from species  $(Z, A)$  and is given by

$$S_n(Z, A) = \Delta_n + \Delta(Z, A - 1) - \Delta(Z, A) \quad (46)$$

From Eqs. (23) and (45), we thus find

$$S_n(Z, A) = \Delta_n - \left[ \frac{\partial \Delta(Z, A)}{\partial A} \right]_Z^- \quad (47)$$

Equivalently, this gives

$$S_n(Z, A) = \left[ \frac{\partial B(Z, A)}{\partial A} \right]_Z^- \quad (48)$$

We see that the neutron-separation energy of a species is the rate of change (by the finite, backward derivative) of the nuclear binding energy of the species with the mass number at constant  $Z$ .

The proton-separation energy of species  $(Z, A)$ , that is, the minimum energy required to remove a proton from species  $(Z, A)$ , is given by

$$S_p(Z, A) = \Delta(Z - 1, A - 1) + \Delta(1, 1) - \Delta(Z, A) \quad (49)$$

This can be recast in our finite-calculus language, for example, by

$$S_p(Z, A) = \Delta(1, 1) - \left[ \frac{\partial \Delta(Z, A)}{\partial Z} \right]_{N=A-Z}^- \quad (50)$$

A related quantity to the neutron-separation energy is the two-neutron-separation energy, which is convenient for comparing nuclei with the same neutron number parity. For species  $(Z, A)$ , it given by

$$S_{2n}(Z, A) = 2\Delta_n + \Delta(Z, A - 2) - \Delta(Z, A) \quad (51)$$

From Eqs. (25) and (45), we see that

$$S_{2n}(Z, A) = \left[ \frac{\partial B(Z, A)}{\partial A} \right]_Z^- + \left[ \frac{\partial B(Z, A - 1)}{\partial A} \right]_Z^- \quad (52)$$

The beta-decay  $Q$  value of a species  $(Z, A)$  is  $Q_\beta(Z, A)$  and is the energy released from the decay that does not go into the rest mass of product particles. It is given by

$$Q_\beta(Z, A) = \Delta(Z, A) - \Delta(Z + 1, A) \quad (53)$$

From Eq. (24) we may identify this as

$$Q_\beta(Z, A) = - \left[ \frac{\partial \Delta(Z, A)}{\partial Z} \right]_A^+ \quad (54)$$

This can also be written

$$Q_\beta(Z, A) = \left[ \frac{\partial B(Z, A)}{\partial Z} \right]_A^+ + (\Delta_n - \Delta(1, 1)) \quad (55)$$

The beta-decay  $Q$  value of a species is thus the rate of change (by the finite, forward derivative) of the binding energy of the species with  $Z$  at constant  $A$  plus the energy a neutron releases in turning into a proton (plus electron).

Normally (and most realistically) one proceeds by measuring or computing nuclear masses (or mass excesses) and then deriving by computing from those masses the needed quantities for r-process calculations such as  $S_n(Z, A)$  or  $Q_\beta(Z, A)$ . In our finite calculus language, this approach is to take finite derivatives of measured or computed quantities.

Our approach will be different. Since we will be beginning with simplified nuclear physics relevant to r-process nucleosynthesis, we will specify quantities like  $S_n$  and  $Q_\beta$  and then integrate to find binding energies and masses. With this approach, we would find, for example, that

$$B(Z, A) = B(Z, \tilde{A}) + \left[ \int_{\tilde{A}}^A S_n(Z, A') dA' \right]^+ \quad (56)$$

or, similarly,

$$\Delta(Z, A) = \Delta(Z, \tilde{A}) + (A - \tilde{A}) \Delta_n - \left[ \int_{\tilde{A}}^A S_n(Z, A') dA' \right]^+ \quad (57)$$

We can also find

$$B(Z, A) = B(\tilde{Z}, A) + \left[ \int_{\tilde{Z}}^Z (Q_\beta(Z', A) - \{\Delta_n - \Delta(1, 1)\}) dZ' \right]^- \quad (58)$$

or, similarly,

$$\Delta(Z, A) = \Delta(\tilde{Z}, A) - \left[ \int_{\tilde{Z}}^Z Q_\beta(Z', A) dZ' \right]^- \quad (59)$$

## VI. SIMPLE NUCLEAR MODEL

We build up our simple nuclear model from prescribed forms for the neutron-separation and beta-decay energies. We begin by assuming smooth variations in these energies that come from macroscopic terms in a nuclear mass model. We then add microscopic terms that contribute non-smooth variations in the nuclear properties.

### A. Macroscopic Mass Model

We construct our macroscopic mass model by assuming smooth variation of the neutron-separation energy in the form

$$S_n(Z, A) = \sum_{k=0}^{k_m} S_k(A_0(Z) - A)^k \quad (60)$$

and the beta-decay energy in the form

$$Q_\beta(Z, A) = \sum_{k=0}^{k_m} Q_k(Z_0(A) - Z)^k \quad (61)$$

Here  $A_0(Z)$  and  $Z_0(A)$  are functions that define the reference curve for our network of nuclei where  $S_n = S_0$  and  $Q_\beta = Q_0$ . We choose a linear reference curve such that

$$A_0(Z) = C_1 + (C_2 + 1)Z \quad (62)$$

and

$$Z_0(A) = \frac{A - C_1}{C_2 + 1} \quad (63)$$

where  $C_1$  and  $C_2$  are constants defining the intercept and slope of the reference curve.

We start from a given species  $(\tilde{Z}, \tilde{A})$ . From Eq. (57), we derive the mass excess  $\Delta(\tilde{Z}, A)$  by integrating over  $A$ . Similarly, with Eq. (59), we derive the mass excess  $\Delta(Z, A)$  by integrating over  $Z$ . Since the relevant quantities will be differences in  $\Delta(Z, A)$ , we choose  $\Delta(\tilde{Z}, \tilde{A}) = 0$  for convenience. From Eq. (40), we thus obtain

$$\begin{aligned} \Delta(Z, A) &= (A - \tilde{A})\Delta_n \\ &- \sum_{k=0}^{k_m} \sum_{p=0}^k (-1)^p \binom{k}{p} \left[ S_k A_0(\tilde{Z})^{k-p} \left\{ B_{p+1}(A+1) - B_{p+1}(\tilde{A}+1) \right\} \right. \\ &\left. + Q_k Z_0(A)^{k-p} \left\{ B_{p+1}(Z) - B_{p+1}(\tilde{Z}) \right\} \right] / (p+1) \end{aligned} \quad (64)$$

We now seek  $Q_\beta$  and  $S_n$  from Eq. (64). We confirm our original definition of  $Q_\beta$ :

$$\begin{aligned} Q_\beta(Z, A) &= \Delta(Z, A) - \Delta(Z+1, A) = - \left[ \frac{\partial \Delta(Z, A)}{\partial Z} \right]_A^+ \\ &= Q_0((Z+1) - Z) + \sum_{k=1}^{k_m} Q_k \sum_{p=0}^k (-1)^p \binom{k}{p} Z_0(A)^{k-p} \frac{B_{p+1}(Z+1) - B_{p+1}(Z)}{p+1} \\ &= Q_0 + \sum_{k=1}^{k_m} Q_k (Z_0(A) - Z)^k \end{aligned} \quad (65)$$

where we used Eq. (43) in simplifying the difference of the Bernoulli polynomials that appears in the expression for  $Q_\beta$ .

For  $S_n(Z, A)$  we find from Eq. (47)

$$\begin{aligned} S_n(Z, A) &= S_0 + \sum_{k=1}^{k_m} \sum_{p=0}^k (-1)^p \binom{k}{p} \left[ S_k A_0(\tilde{Z})^{k-p} A^p \right. \\ &\left. + Q_k \left\{ Z_0(A)^{k-p} - Z_0(A-1)^{k-p} \right\} \frac{B_{p+1}(Z) - B_{p+1}(\tilde{Z})}{p+1} \right] \end{aligned} \quad (66)$$

The neutron-separation energy should not depend on the choice of  $\tilde{Z}$ . By eliminating this dependence, we are able to derive in Appendix C the following relation between  $Q_k$  and  $S_k$  for  $k \geq 1$ :

$$Q_\ell = \frac{1}{\beta_\ell^{(\ell)}} \left[ \sum_{k=\ell}^{k_m} S_k \alpha_\ell^{(k)} - \sum_{k=\ell+1}^{k_m} Q_k \beta_\ell^{(k)} \right] \quad (67)$$

where

$$\alpha_\ell^{(k)} = \binom{k}{k-\ell} C_1^{k-\ell} (C_2 + 1)^\ell \quad (68)$$

and

$$\beta_\ell^{(k)} = (-1)^{k-1} \frac{k!}{\ell!} \sum_{j=1}^{k-\ell+1} \frac{[(C_1+1)^j - C_1^j]}{(k-\ell-j+1)! j! (C_2+1)^j} B_{k-\ell-j+1} \quad (69)$$

and  $C_1$  and  $C_2$  are the coefficients defining the network reference curve.

From Eq. (67), we may determine  $Q_k$  for  $k \geq 1$  from the already specified  $S_k$ 's and  $C_1$  and  $C_2$ . We begin with  $\ell = k_m$ , from which we find  $Q_{k_m} = S_{k_m} \alpha_{k_m}^{(k_m)} / \beta_{k_m}^{(k_m)} = (-1)^{k_m-1} (C_2 + 1)^{k_m+1} S_{k_m}$ . With knowledge of  $Q_{k_m}$ , we then proceed to find  $Q_{k_m-1}$ . In this way, we iterate down to  $Q_1$ . For example, if  $k_m = 2$ , then  $Q_2 = -(C_2 + 1)^3 S_2$ . Then  $Q_1 = (C_2 + 1)^2 (S_1 + S_2 C_2)$ .  $S_0$  and  $Q_0$  are free parameters that must be specified.

## B. Microscopic Mass Terms

Single-particle effects contribute to the final neutron-separation energies and beta  $Q$  values of nuclei. One single-particle effect is nucleon pairing, which accounts for extra nuclear binding in the nucleus when the spin-1/2 nucleons pair up. Shell effects are another single-particle phenomenon that arises from coupling of nucleons in their single-particle orbitals in the nuclear potential. We can account for these effects in our simple model.

First, it is useful to define three functions of integer argument  $x$ . These are

$$\Sigma(x) = \begin{cases} 1 & \text{if } x \text{ is even} \\ -1 & \text{if } x \text{ is odd} \end{cases} \quad (70)$$

$$\Theta(x) = \begin{cases} 1 & \text{if } x > 0 \\ 0 & \text{if } x \leq 0 \end{cases} \quad (71)$$

$$\Pi(x) = \begin{cases} 0 & \text{if } x \text{ is even} \\ 1 & \text{if } x \text{ is odd} \end{cases} \quad (72)$$

Eq. (70) is a sign function, Eq. (71) is a step function, and we term Eq. (72) the Pi function.

With these functions, our  $S_n(Z, A)$  with shell and pairing effects is

$$S_n(Z, A) = S_n^{(0)}(Z, A) + \delta_n \Sigma(A - Z) - \sum_s C_s \Theta(A - Z - N_s) \quad (73)$$

where  $S_n^{(0)}$  is the separation function without shell and pairing effects [Eq. (60)]. The first correction,  $\delta_n \Sigma(A - Z)$ , where  $\delta_n$  is a constant, is the pairing correction. It increases or decreases the separation energy by a constant amount depending on whether the neutron number of the nucleus is even or odd, such that the neutrons are fully paired up or not. The second correction is the shell correction. It is a sum over neutron shells ( $s$ ). As the neutron number of the nucleus increases one unit past a magic number  $N_s$ , the neutron-separation energy drops by a uniform amount given by the constant  $C_s$ .

We now compute  $Q_\beta(Z, A)$  with pairing and shell effects. From Eqs. (46), (49), and (53), we may note that

$$Q_\beta(Z, A) = S_p(Z + 1, A + 1) - S_n(Z, A) + (\Delta(1, 1) - \Delta_n) \quad (74)$$

The full beta decay energy is

$$Q_\beta(Z, A) = Q_\beta^{(0)}(Z, A) - \delta_n \Sigma(A - Z) - \delta_p \Sigma(Z) - \sum_t C_t \Theta(Z + 1 - Z_t) + \sum_s C_s \Theta(A - Z - N_s) \quad (75)$$

where  $Q_\beta^{(0)}(Z, A)$  is the beta decay energy without the shell and pairing effects.  $\delta_p$  and  $C_t$  are the paring and shell corrections for protons.

Finite integration yields

$$\left[ \int_{x_0}^x \Sigma(x') dx' \right]^+ = \sum_{x_0+1}^x \Sigma(x') = \Sigma(x_0 + 1) \Pi(x - x_0) = -\Sigma(x_0) \Pi(x - x_0) \quad (76)$$

and

$$\left[ \int_{x_0}^x \Theta(x' - x_s) dx' \right]^+ = \sum_{x_0+1}^x \Theta(x' - x_s) = \Theta(x - x_s) \sum_{x_m+1}^x (x')^0 = \Theta(x - x_s) (x - x_m) \quad (77)$$

where  $x_m$  is the maximum of  $x_0$  and  $x_s$ . With these results and the full expressions of  $S_n$  and  $Q_\beta$ , we can get the mass of any species ( $Z, A$ ) by finite integration over  $A$  of Eq. (73) and then over  $Z$  of Eq. (75)

$$\begin{aligned} \Delta(Z, A) = & \Delta^{(0)}(Z, A) + \delta_n (\Pi(A - Z) - 1) + \delta_p (\Pi(Z) - 1) \\ & + \sum_s C_s \Theta(A - Z + 1 - N_s) (A - Z + 1 - N_m) + \sum_t C_t \Theta(Z - Z_t) (Z - Z_m) \end{aligned} \quad (78)$$

The proton-separation energy can be derived as

$$\begin{aligned}
S_p(Z, A) &= \Delta(1, 1) + \Delta(Z - 1, A - 1) - \Delta(Z, A) \\
&= S_p^{(0)}(Z, A) + \delta_p \Sigma(Z) - \sum_t C_t \Theta(Z - Z_t)
\end{aligned}
\tag{79}$$

where  $S_p^{(0)}(Z, A)$  is the separation energy without the pairing and shell effects.

Fig. 6 compares neutron-separation energies from our model with those derived from the REACLIB V2.2 database [35]. While our model cannot reproduce subtle local variations (e.g.  $N$  around 85 in this figure) in the separation energies of the real data or values from the detailed microscopic-macroscopic nuclear model in the database, it does capture many of the key features, like even-odd staggering and the sharp drops at neutron closed-shells.

### C. Nuclear Partition Function

The nuclear partition function  $G(Z, A)$  accounts for the number of states available to a nuclear species  $(Z, A)$  among the nuclear levels within the nucleus. In what follows, it will be convenient to assume in our model that the nuclear partition function scales inversely with the 3/2 power of the species mass  $m(Z, A)$ :

$$G(Z, A)m(Z, A)^{3/2} = C \tag{80}$$

where  $C$  is a constant independent of  $Z$  and  $A$ .

The assumption in Eq. (80) is a matter of convenience.  $m(Z, A)$  scales with  $A$  and  $G(Z, A)$  scales with the ground-state spin of the species and the number of accessible energy levels at the given temperature, which can vary by factors of several from species to species. This is illustrated in Fig. 7, which shows this factor and the separate mass and partition function factors. There is clear variation over the mass number for the given isotopic chain. Nevertheless, these quantities enter as ratios over a limited range in mass number [Eq. (13)]. The resulting ratio varies much less than that of the other quantities in the abundance expression, so the approximation in Eq. (80) is sufficiently accurate for our purposes of delineating the main features of equilibrium isotopic abundance distributions, though we return to this issue in §VIII.

## VII. ISOTOPIC ABUNDANCES IN $(n, \gamma) - (\gamma, n)$ EQUILIBRIUM

We now consider isotopic abundances in  $(n, \gamma) - (\gamma, n)$  equilibrium in our simple nuclear physics model. With the assumption of Eq. (80), the equilibrium isotopic abundance distribution is

$$\frac{Y(Z, A)}{Y(Z, A_0)} = \exp \left\{ \frac{1}{kT} \left[ \int_{A_0}^A [\mu'_n + S_n(Z, A')] dA' \right]_Z^+ \right\} \quad (81)$$

With Eq. (41) and Eq. (73), this can be written:

$$\begin{aligned} \frac{Y(Z, A)}{Y(Z, A_0)} = & \exp \left\{ \frac{1}{kT} \left[ (A - A_0)\mu'_n + \sum_{k=0}^{k_m} (-1)^k S_k \frac{B_{k+1}(A - A_0 + 1) - B_{k+1}(1)}{k + 1} \right] \right\} \\ & \times \exp \left\{ -\frac{\delta_n}{kT} \Sigma(A_0 - Z) \Pi(A - A_0) \right\} \exp \left\{ -\frac{\sum_s C_s \Theta(A - Z - N_s)(A - Z - N_m)}{kT} \right\} \end{aligned} \quad (82)$$

This equation is the basis for our subsequent discussion.

### A. Constant $S_n$ ( $[k_m, \delta_n, C_s] = [0, 0, 0]$ )

Constant neutron-separation energy, though physically implausible, means that no nuclear species preferentially binds neutrons. In our simple model, this corresponds to  $k_m = 0$ ,  $\delta_n = 0$  and  $C_s = 0$  in Eq. (73), in which case Eq. (82) becomes

$$\frac{Y(Z, A)}{Y(Z, A_0)} = \exp \left\{ \frac{1}{kT} (\mu'_n + S_0) (A - A_0) \right\} \quad (83)$$

The chemical potential of the neutrons less the rest mass,  $\mu'_n$ , is a negative quantity for non-degenerate matter. This means that the isotopic abundances are either exponentially growing or declining with mass number depending on whether  $\mu'_n + S_0$  is a positive or negative quantity. If the quantity is positive, it is thermodynamically favorable for nuclei to capture more neutrons. As neutrons disappear, however,  $\mu'_n$  becomes increasingly negative; thus, captures would continue until  $\mu'_n + S_0 = 0$ . In this case, the isotopic pattern would be flat with  $A$ . No species in the chain would be favored over any other.

If  $\mu'_n + S_0$  is negative, nuclei would tend to disintegrate neutrons, which would tend to increase  $\mu'_n$  in the positive direction. This would occur until  $\mu'_n + S_0 = 0$ . The isotopic abundance pattern for constant  $S_n$ , then, would tend to be flat, unless limits on the network prevent the neutron captures or disintegrations that would establish the flat pattern. If such

limits exist, the isotopic pattern would be a rising or declining exponential, as previously noted.

**B. Linear  $S_n$  ( $[k_m, \delta_n, C_s] = [1, 0, 0]$ )**

For linear  $S_n$ ,  $k_m = 1$ ,  $\delta_n = 0$  and  $C_s = 0$  in Eq. (73). In this case, Eq. (82) becomes (see Table III)

$$\frac{Y(Z, A)}{Y(Z, A_0)} = \exp \left\{ \frac{1}{kT} \left[ \left( \mu'_n + S_0 - \frac{S_1}{2} \right) (A - A_0) - \frac{S_1}{2} (A - A_0)^2 \right] \right\} \quad (84)$$

This may be written

$$\frac{Y(Z, A)}{Y(Z, A_0)} = \exp \left\{ \frac{(\bar{A} - A_0)^2}{2\sigma^2} \right\} \exp \left\{ -\frac{(A - \bar{A})^2}{2\sigma^2} \right\} \quad (85)$$

where

$$\bar{A} = \frac{\mu'_n + S_0}{S_1} - \frac{1}{2} + A_0 \quad (86)$$

and where

$$\sigma = \sqrt{\frac{kT}{S_1}} \quad (87)$$

For the linear  $S_n$ , the isotopic abundance distribution in  $(n, \gamma) - (\gamma, n)$  equilibrium is a Gaussian centered at  $\bar{A}$  and with width  $\sigma$ . The location of the abundance maximum is governed by the quantity  $\mu'_n + S_n$ . Again, for non-relativistic, non-degenerate neutrons,  $\mu'_n$  is negative, and, as the neutron number density increases,  $\mu'_n$  is a smaller negative number. This causes the maximum to shift higher in  $A$  at a constant temperature. By Le Chatlier's Principle, the equilibrium would respond to an increase in the neutron number density by trying to counter that increase. It would do so by having the nuclei capture neutrons, which would decrease the neutron abundance. The reverse is true if the neutron number density decreases.

Similarly, at constant neutron number density,  $\bar{A}$  will increase with decreasing temperature. Lower temperature means lower neutron disintegration rates, which tends to drive the abundance distribution toward more neutron-rich species. The neutron captures release energy since the capture reactions are exothermic. This tends to deposit energy locally, which counters the temperature decrease, again in agreement with Le Chatelier's Principle.

The shift in the location of the maximum in the abundance distribution is also governed by the slope. A shallower slope leads to a bigger change in  $\bar{A}$  with change in  $\mu'_n$ . This is due

to the more equal binding of neutrons in nuclei so that a bigger change in mass number is needed to realign the binding of neutrons inside and outside nuclei.

The width of the abundance distribution scales with the square root of the temperature. As the temperature declines, the width of the abundance distribution becomes sharper. The width also scales inversely with the square root of the slope of  $S_n$ . A shallower slope means the binding of neutrons in nuclei is more equal across mass numbers, so the abundance distribution will be broader. An example of the equilibrium isotopic abundance distribution for the linearly declining neutron-separation energy is shown in Fig. 8.

### C. Linear $S_n$ and Pairing ( $[k_m, \delta_n, C_s] = [1, \delta_n, 0]$ )

For a linear neutron-separation energy that includes pairing, application of Eq. (76) to Eq. (82) yields

$$\frac{Y(Z, A)}{Y(Z, A_0)} = \exp \left\{ \frac{(\bar{A} - A_0)^2}{2\sigma^2} \right\} \exp \left\{ -\frac{(A - \bar{A})^2}{2\sigma^2} \right\} \exp \left\{ -\frac{\delta_n}{kT} \Sigma(A_0 - Z) \Pi(A - A_0) \right\} \quad (88)$$

with  $\bar{A}$  and  $\sigma$  as defined in Eqs. (86) and (87), respectively. The pairing term adds a multiplicative factor on the abundance that depends on the parity of  $A - A_0$ . If  $A - A_0$  is even, the abundance is unchanged from purely linear neutron-separation energy case. If  $A - A_0$  is odd, the abundance is increased or decreased from the linear case depending on the parity of  $A_0 - Z$ , the neutron number of the first species in the chain. If  $A_0 - Z$  is even, odd  $A - A_0$  corresponds to odd  $A - Z$ , and the abundance is decreased from the baseline linear case. If  $A_0 - Z$  is odd, odd  $A - A_0$  corresponds to even  $A - Z$ , and the abundance is increased from the baseline linear case.

Fig. 9 shows a linear neutron-separation energy with pairing and the resulting normalized equilibrium isotopic abundance. It is evident that the isotopic abundance pattern jumps between two Gaussians (an even neutron-number gaussian and an odd neutron-number gaussian). The size of the jumps in the abundance increases with larger pairing energy  $\delta_n$  and with decreasing temperature.

#### D. Linear $S_n$ and Shell effect ( $[k_m, \delta_n, C_s] = [1, 0, C_s]$ )

For a linear neutron-separation energy function including the shell effect, application of Eq. (77) to Eq. (82) yields

$$\frac{Y(Z, A)}{Y(Z, A_0)} = \exp\{\Phi(Z, A)\} \exp\left\{\frac{(\bar{A} - A_0)^2}{2\sigma^2}\right\} \exp\left\{-\frac{(A - \bar{A})^2}{2\sigma^2}\right\} \quad (89)$$

where  $\bar{A}$  and  $\sigma$  are defined in Eq. (86) and Eq. (87).

$$\Phi(Z, A) = -\frac{1}{kT} \sum_s C_s \Theta(A - Z - N_s)(A - Z - N_m) \quad (90)$$

Here  $N_m$  is the maximum of  $N_s$  and  $A_0 - Z$ . If the value  $A - Z = N$  is smaller than the first closed-shell,  $\exp\{\Phi(Z, A)\} = 0$ , the abundance keeps its initial form. If  $N \in [N_j, N_{j+1}]$ , with  $j$  the  $j^{\text{th}}$  closed-shell, the abundances in shell  $j$  will be its initial form times  $\exp\{\Phi(Z, A)\}$ , which can also be written as

$$\frac{Y_j(Z, A)}{Y(Z, A_0)} = \exp\{\phi_j\} \exp\left\{\frac{(\bar{A}_j - A_0)^2}{2\sigma^2}\right\} \exp\left\{-\frac{(A - \bar{A}_j)^2}{2\sigma^2}\right\} \quad (91)$$

The  $\bar{A}_j$  is the peak position between shell  $j$  and  $j + 1$ .

$$\bar{A}_j = \bar{A} - \frac{\sum_{s=1}^j C_s \Theta(A - Z - N_j)}{S_1} \quad (92)$$

So, if the neutron number is larger than a neutron closed-shell, the isotopic abundance peak position will shift to the left by a factor of  $C_s/S_1$ .

The  $\phi_j$  is fixed between shell  $j$  and  $j + 1$  if we keep the temperature constant.

$$\phi_j = -\frac{1}{kT} \sum_{s=1}^j C_s (A_0 - Z - N_m) \quad (93)$$

Therefore, if  $A - Z$  in an isotope chain is between  $N_j$  and  $N_{j+1}$ , the abundance distribution will follow a new Gaussian distribution with abundance maximum at  $\bar{A}_j$ , which can be seen in Fig. 10. However, if the value of  $A - Z$  is between  $N_{j-1}$  and  $N_{j+1}$ , the abundance distribution before  $N_j$  follows a Gaussian curve  $Y_{j-1}(Z, A)$ , while it changes to another Gaussian  $Y_j(Z, A)$  once the value of  $A - Z$  crosses  $N_j$ . The closed-shell is where this transition occurs, which means  $Y_{j-1}(Z, A) = Y_j(Z, A)$  when  $A - Z = N_j$ . This behavior is shown in Fig. 11, which illustrates how the equilibrium abundance distribution is affected by magic number  $N_j = 50$  or by  $N_j = 82$ .

### E. Quadratic $S_n$ ( $[k_m, \delta_n, C_s] = [2, 0, 0]$ )

In the neutron-separation energy curve plotted from the REACLIB V2.2 database Fig. 6, we notice that when  $S_n$  drops, there is a small curvature. Inspired by this feature, we need to consider a quadratic  $S_n$ . This corresponds to  $k_m = 2$  in Eq. (60), in which case Eq. (82) becomes (see Table III).

$$\frac{Y(Z, A)}{Y(Z, A_0)} = \exp \left\{ \frac{1}{kT} \left[ (S_0 + \mu'_n - \frac{S_1}{2} + \frac{S_2}{6})(A - A_0) - \frac{S_1 - S_2}{2}(A - A_0)^2 + \frac{S_2}{3}(A - A_0)^3 \right] \right\} \quad (94)$$

If we expand Eq. (94) in  $\bar{A}'$  as we did in Eq. (85), the new peak position  $\bar{A}'$  can be written as:

$$\bar{A}' \approx \frac{1}{1 - \frac{S_2}{S_1}} \left\{ \bar{A} - A_0 + \frac{S_2}{S_1} \left[ (\bar{A} - A_0)^2 + \frac{1}{6} \right] \right\} + A_0 \quad (95)$$

The new standard deviation:

$$\sigma = \sqrt{\frac{kT}{S_1 - S_2(1 + 2(\bar{A}' - A_0))}} \quad (96)$$

From Eq. (95) and Eq. (96), we expect that the peak position of this new abundance distribution shifts to a higher mass number  $A$ . At the same time, the width of this distribution would be broader than the linear case. This new abundance distribution is presented in Fig. 12. It is clear that the slight curvature in  $S_n$  pushes the intersection of  $S_n$  and  $-\mu'_n$  slightly to the right. This intersection movement leads to the right movement of abundance peak in the lower panel, which is consistent with our Eq. (95). If we compare both sides' deviations, we find that the difference on the left is smaller than the right, which means the quadratic term also makes the abundance distribution have a positive skew. This is reasonable, since from Eq. (82), the abundance is affected by the summation of  $S_n$  and  $\mu'_n$ . If  $S_n + \mu'_n$  in the linear and quadratic cases are close, the deviation is slight, otherwise, the deviation is large.

### F. Quadratic $S_n$ with Pairing and Shell effects ( $[k_m, \delta_n, C_s] = [2, \delta_n, C_s]$ )

The separation energy is not only determined by the value of  $S_k$  but also affected by both the shell and pairing effects. Now we include both effects in the quadratic separation function, which makes our separation energy data closer to the database. Integrating this

well-defined separation energy function, we can find the final abundance expression; its distribution curve is shown in Fig. 13.

From the upper part of each panel in Fig. 13, we can see the separation energy decreases when the neutron number increases, and the decreasing is steep when it encounters neutron closed shells. We can also notice a slight curvature when  $S_n$  drops, which is the quadratic term's contribution. The intersection of  $S_n$  and  $\mu'_n$  is the abundance peak in the lower part of each panel. From the lower part of each panel in Fig. 13, We can see the spikes on the Gaussian distribution due to the pairing effect. Moreover, the abundance ratio curve transfers from one Gaussian to another Gaussian when  $N$  (or  $A - Z$ ) crosses the closed shell 50 and 82, which can be seen from the left panels. The right panels demonstrates a full Gaussian since  $N$  does not cross any closed-shell.

### VIII. SPIKES IN THE SEPARATION-ENERGY CURVE AND A GENERAL APPROACH TO INFERRING EQUILIBRIUM ABUNDANCES

In this section we consider modifications to the equilibrium abundances when the linear separation energy curve is modified by addition of an extra energy  $\epsilon$  at mass number  $A_\epsilon$ . We write

$$S_n(Z, A) = S_0 + S_1(A_0 - A) + \epsilon\delta(A - A_\epsilon) \quad (97)$$

with the finite delta function  $\delta(x - y) = 1$  if  $x = y$  and  $\delta(x - y) = 0$  otherwise. We then find

$$\left[ \int_{x_0}^x \delta(x' - y) dx' \right]^+ = \Theta(x - y + 1)\Theta(y - x_0) \quad (98)$$

In this case, the abundance function is

$$\frac{Y(Z, A)}{Y(Z, A_0)} = \left( \frac{Y(Z, A)}{Y(Z, A_0)} \right)^{(0)} \times \left\{ \begin{array}{l} \exp(0); \quad A < A_\epsilon \\ \exp\left(\frac{\epsilon}{kT}\right); \quad A \geq A_\epsilon \end{array} \right\} \quad (99)$$

Where the  $\left( \frac{Y(Z, A)}{Y(Z, A_0)} \right)^{(0)}$  is the abundance for a linear  $S_n$  in Eq. (85). Therefore, the abundance curve does not change when mass number  $A$  is less than  $A_\epsilon$ , but transfers to another Gaussian that is a factor of  $\exp(\frac{\epsilon}{kT})$  larger or smaller than its initial distribution depending on the value of  $\epsilon$ . Similarly, if two continuous spikes appear in the neutron-separation energy, the abundances curve will transfer twice. Those behaviors are shown in Fig. 14. From part (a) of Fig. 14, we can see a positive spike in  $S_n$  in the upper panel and a transformation

from one Gaussian to another Gaussian curve at the spike position ( $N = 70$ ) in the lower panel. From part (b) of Fig. 14, the upper panel shows the  $S_n$  with two continuous negative spikes. Therefore, the corresponding abundances curve transfers to one Gaussian after the first spike ( $N = 51$ ) and then transfer to another Gaussian after the second negative spike ( $N = 52$ ).

The idea of spikes on top of a separation energy curve decreasing linearly with mass number in fact provides a general way of inferring the abundance distribution in  $(n, \gamma) - (\gamma, n)$  equilibrium. Add to the linearly decreasing separation function a series of spikes with the necessary magnitude at the appropriate mass numbers. The abundance curve will shift from the Gaussian resulting from the original separation energy curve to other Gaussians either above or below the first according to the spike function prescription. For example, add the spike function  $\epsilon(A) = S_1(A - \bar{A})$  to the linear function  $S_n = S_0 + S_1(A_0 - A)$ . This spike function adds continuously decreasing negative spikes before the peak position  $\bar{A}$  and adds continuously increasing positive spikes after  $\bar{A}$ . The result is a flat separation energy curve  $S_n = S_0 + S_1(A_0 - \bar{A})$  and an abundance distribution that shifts to lower-lying Gaussians as  $A$  increases towards  $\bar{A}$  and to higher-lying Gaussians as  $A$  increases past  $\bar{A}$  with the result in Eq. (83). We may also view the microscopic terms in Eq. (73) in terms of spikes. The pairing term is an alternating set of spikes with magnitude  $\delta_n$  and sign determined by the parity of the neutron number. The abundance distribution for the originally linearly decreasing separation energy then bounces between two Gaussians, as shown in Fig. 9. The shell term is a series of spikes with magnitude given by a sum on the shell strengths  $C_s$  for the shells crossed. These spikes are subtracted from the original smooth separation energy. This correction makes the abundance curve jump to a set of decreasing Gaussian curves which can be seen in Fig. 15. The resulting abundance curve after the neutron magic number is in fact a new Gaussian, as noted in Eq. (91). Fig. 16 shows the effect of two shell crossings. The spikes after the second shell crossing are twice as large in magnitude as the spikes just after the first shell crossing. As a last example, a quadratic neutron-separation energy is equivalent to a linear  $S_n$  with the spike function  $\epsilon(A) = S_2(A - A_0)^2$ . This correction adds increasing spikes in  $S_n$  when the mass number increases and therefore skews the abundance curve because it is shifting to increasingly displaced Gaussians. This idea naturally extends to higher orders in the power-series expansion of the separation energy.

The procedure for determining a general abundance curve then is to add an appropriate

spike function to the linearly decreasing neutron-separation energy curve. The spikes define the displacement of Gaussians away from the original Gaussian due to the linear separation energy, and each spike magnitude may depend on the mass number locating the spike. The abundance curve is the result of steps from the Gaussian for one mass number to the Gaussian for the next mass number.

It is worth noting here that should species  $(Z, A)$  have an unequilibrated isomeric state such that the isomeric state is effectively a separate species from the ground state, the neutron-separation energy for the isomer will be lowered relative to that for the ground state of  $(Z, A)$ . As a result, the neutron-separation energy curve versus mass number for element  $Z$  would show a spike down at  $(Z, A)$  for the isomer relative to the ground state. Similarly, there would be a spike up of the same magnitude at  $(Z, A + 1)$ . The abundance curve including the isomer would thus show a notch at  $(Z, A)$  relative to the curve for the ground state for  $(Z, A)$ . The spike down in the neutron-separation energy curve versus mass number shifts the abundance to a lower curve while the spike up shifts the curve back up to the original abundance curve. This creates the notch in a fashion analogous to pairing.

We may finally return to the question of the prefactor on the abundances that we have previously neglected through the approximation in Eq. (80). If we do not make this approximation, we can see from Eq. (13) that we effectively add to the neutron-separation energy a quantity

$$\frac{3}{2}kT \ln \left[ \frac{m(Z, A)}{m(Z, A - 1)} \right] + kT \ln \left[ \frac{G(Z, A)}{G(Z, A - 1)} \right] \approx \frac{3}{2} \frac{kT}{A} + \epsilon_G(Z, A) \quad (100)$$

where we have used the fact that  $m(Z, A)$  scales with  $A$  and  $A \gg 1$ , and we have defined

$$\epsilon_G(Z, A) = kT \ln \left[ \frac{G(Z, A)}{G(Z, A - 1)} \right] \quad (101)$$

From Eq. (B6), inclusion of the prefactor would then result in the isotopic abundances in Eq. (81) being multiplied by the slowly varying factor  $\exp \left\{ \frac{3}{2} (H_{A,1} - H_{A_0,1}) \right\}$  times modifications given by the spike factor  $\epsilon_G(Z, A)$ .

## IX. APPLICATION TO REALISTIC NUCLEAR MODELS

In this section, we analyze the effects of realistic, or at least more traditional, nuclear physics models on  $(n, \gamma) - (\gamma, n)$  equilibrium abundances in terms of the simple model we

have thus far presented. The goal is to illustrate ways nuclear physicists can use our analysis to interpret how their own nuclear data affects equilibrium abundance curves.

### A. Liquid-Drop Model

The equilibrium abundance formula with  $k = 2$  is written in Eq. (94). From Eq. (20), we know the value of  $S_k$  depends the liquid-drop model parameters  $a_S, a_C, a_A, a_V$ ; thus, these parameters play the crucial role in determining the equilibrium isotopic abundance pattern. We explore the effect of fractional variation of those nuclear physics coefficients on the value of  $S_k$  and the consequences for the equilibrium abundance patter. We choose to analyze  $Z = 50$  and  $A_0 = 100$ . For reference values of the liquid-drop model parameters, we use reference values  $a_S = 17.8$  MeV,  $a_C = 0.711$  MeV, and  $a_A = 23.7$  MeV [36]. These parameters result in power-series coefficients  $S_0 = 14.47$  MeV,  $S_1 = 0.4825$  MeV, and  $S_2 = 0.0073$  MeV.

Fig. 17 shows the effect of varying  $a_S$ , the surface term coefficient while holding other parameters fixed. An increase in  $a_S$  causes  $S_0$ ,  $S_1$ , and  $S_2$  all to decrease, but the largest effect is in  $S_0$ . Because  $S_1$  and  $S_2$  remain nearly constant and  $S_2$  is small, the equilibrium abundance curve maintains its nearly Gaussian shape. The decrease in  $S_0$  with increasing  $a_S$  causes the peak of the abundance curve to move to lower mass number, as expected from Eq. (86).

When the Coulomb term coefficient is increased, the power-series coefficients all increase, as seen in Fig. 18. From Eq. (86), an increase in  $S_0$  shifts  $\bar{A}$  to larger value while an increase in  $S_1$  does the reverse. The magnitude of the change in  $S_0$  is larger than that in  $S_1$ , so  $\bar{A}$  does move to larger vslue for the increase in  $a_C$ , but the change in peak position is not as pronounced as in Fig. 17 because in the latter case, the magnitude of the change in  $S_0$  is greater and there is no compensating effect from  $S_1$ . The slight increase in  $S_2$  adds more of a positive skew for larger  $a_C$ , but that effect is hardly visible in the present case.

The change in the asymmetry term  $a_A$  produces some dramatic effects as seen from Fig. 19. From our particular choice of  $Z$  and  $A_0$ ,  $S_0$  is independent of  $a_A$ . The fractional changes in  $S_1$  and  $S_2$  with  $a_A$  variations are identical. The increase in  $S_1$  with increasing  $a_A$  causes the peak equilibrium abundance to shift to lower mass and narrow, as expected; however, the increase in  $S_2$  with increasing  $a_A$  tends to shift the abundance peak to higher mass

number, so the increase in  $S_2$  tends to compensate the decrease in peak mass number and slows the shift to lower mass with increasing  $a_A$ .

## B. Detailed Nuclear Data

We now turn to the detailed nuclear data in the REACLIB V2.2 database [35]. We analyze the equilibrium abundance curves for selected isotope chains in order to illustrate the application of our treatment to realistic nuclear models.

Fig. 20 shows data for  $Z = 70$ . When  $-\mu'_n$  crosses a spike, we see that the equilibrium abundance curve shifts up, as expected from Eq. (99) we know the abundance curve does not change when mass number  $A$  is less than  $A_\epsilon$ , but transfers to another Gaussian that is a factor of  $\exp(\frac{\epsilon}{kT})$  larger than its initial distribution. At a somewhat lower  $-\mu'_n$ , as shown in Fig. 21, when  $-\mu'_n$  intersects the  $S_n$  curve where the curve is flat leads to a flat abundance distribution (modulated by pairing spikes), as expected from Eq. (83).

From Eq. (88), we know that the pairing correction in the isotopic abundance is determined by the parity of the neutron number, the value  $\delta_n$  and the temperature  $T$ . Fig. 22 shows results for  $Z = 55$ . The  $S_n$  curve has distinctive  $\delta_n$ 's before and after the closed neutron shell at  $N = 82$ . Two different  $-\mu'_n$  are presented, both computed at  $T_9 = 2$  but at different neutron densities so that the  $-\mu'_n$  curves intersect  $S_n$  in different shells. Because the shells have different  $\delta_n$ , the jaggedness is different for the two resulting equilibrium abundance curves. Fig. 23 shows results for a given  $-\mu'_n$  for  $Z = 68$ . Here the pairing  $\delta_n$  shifts within the shell so that the left half of the resulting equilibrium abundance curve shows a jagged distribution due to the large  $\delta_n$ , while the right half is less jagged due to the smaller  $\delta_n$ .

Temperature also affects the pairing correction. Decreasing temperature enhances the pairing effect on the abundance distribution. Fig. 24 shows results for  $Z = 55$  for a fixed neutron density but for two different temperatures,  $T_9 = 3$  and  $T_9 = 1$ . The higher temperature gives an abundance distribution at lower mass number than for the lower temperature case, as expected. The lower temperature distribution is more jagged than the higher temperature case despite the smaller pairing energy  $\delta_n$  for  $S_n$  at the peak mass number for the lower temperature case. This is of course due to the pairing term exponential in Eq. (88) that depends on  $\delta_n/kT$ .

These examples certainly do not exhaust all possible analyses one may make of the expected equilibrium isotopic abundance curves from detailed  $S_n$  curves. Nevertheless, they do give a sense of how our analysis can be applied to such realistic nuclear models.

## X. $(p, \gamma) - (\gamma, p)$ EQUILIBRIUM

Though the production sites for r-process elements are not yet fully determined due to difficulties in computing the complete dynamics of the extreme astrophysical environments in which the nucleosynthesis occurs, neutrino-driven winds are typically considered as plausible candidates [3, 37] for at least some of the r-process species. However, if the ejecta is proton-rich (electron fraction  $Y_e > 0.5$ ), especially due to neutrino-nucleus interactions during the expansion of the material, r-process nucleosynthesis is unlikely to occur. The matter in these proton-rich winds is initially hot and fully dissociated [38]. When the matter expands and cools, it will freeze out from nuclear statistical equilibrium (NSE) to quasi-equilibrium (QSE). At this process continue, nuclei up to  $^{56}\text{Ni}$  and even  $^{64}\text{Ge}$  are formed once the temperature is lower than 3 GK. When the temperature decreases to 3 GK-1.5 GK, a proton capture process occurs, which creates heavy elements that cannot be formed by either s- and r-process, and  $\beta^+$  decays shift the flow from one value of  $N$  to the next. During this phase, neutrinos can enhance the production of neutrons which facilitates the nuclear flow to mass  $A > 64$  in what is termed the  $\nu p$  process [39].  $(p, \gamma) - (\gamma, p)$  equilibrium is a crucial phase in determining the final p-nuclei abundances, which is similar to the  $(n, \gamma) - (\gamma, n)$  phase discussed above. Based on our simple nuclear model, the isotonic (a fixed neutron number  $N$  with varying proton number  $Z$ ) abundance pattern in each isotonic chain also has features analogous to the isotopic chain abundance features of  $(n, \gamma) - (\gamma, n)$  equilibrium. The only difference between these two phases is that the isotopic abundance is determined by the neutron-separation energy  $S_n$ , while the isotonic abundance is determined by the proton-separation energy  $S_p$ . The corresponding abundance distribution for isotonic chain  $N$  is

$$\frac{Y(Z, A = Z + N)}{Y(Z_0, A_0 = Z_0 + N)} = \frac{G(Z, A = Z + N)}{G(Z_0, A_0 = Z_0 + N)} \left[ \frac{m(Z, A = Z + N)}{m(Z, A_0 = Z_0 + N)} \right]^{3/2} \times \exp \left\{ \frac{1}{kT} \left[ \int_{Z_0}^Z [\mu'_p + S_p(Z', A' = Z' + N)] dZ' \right]_N^+ \right\} \quad (102)$$

To explore the  $(p, \gamma) - (\gamma, p)$  equilibrium in such expansions, we ran a  $\nu p$ -process network calculation with the same network code used for our previously discussed r-process calculation. The matter began at  $T_9 = 10$  and a density of  $\rho = 1.68 \times 10^7$  g/cc. The density decreased exponentially on an e-folding timescale of 0.2 seconds. We included neutrino-nucleus interactions reactions [30] and followed the expansion for 10 seconds. Fig. 25 shows the chemical potential offset of a subset of species in the range from Cl ( $Z = 17$ ) to Zr ( $Z = 40$ ) in the network at time 0.914 s into the expansion. The network now, in each isotonic chain, is in the  $(p, \gamma) - (\gamma, p)$  equilibrium phase of the expansion such that the species are in equilibrium under exchange of protons, but movement from one isotonic chain to another is slow. Similar to the  $(n, \gamma) - (\gamma, n)$  equilibrium phase, the relative isotonic abundance pattern also peaks at the intersection of  $S_p(Z, A)$  and  $-\mu'_p$ . The pairing term of  $S_p$  in Eq. (79) adds alternating spikes in the abundance curve, which can be seen from the right panel of Fig. 26. It is clear that much of our analysis for  $(n, \gamma) - (\gamma, n)$  equilibrium carries over to the  $(p, \gamma) - (\gamma, p)$  equilibrium phase of proton-rich expansions.

## XI. CONCLUSION

We have studied the effects of nuclear physics inputs on  $(n, \gamma) - (\gamma, n)$  equilibrium isotopic abundances. To do so, we reversed the usual route of determining key nuclear physics properties for r-process nucleosynthesis, namely, neutron-separation energies and the beta-decay Q values by finite differentiating experimentally or theoretically derived nuclear masses. We instead developed our own nuclear model by setting the key properties to mathematically convenient forms and then finite integrating them to derive the nuclear masses. This allowed us to compute equilibrium isotopic abundances with well-defined input.

Up to slowly varying prefactors depending on ratios of masses and nuclear partition functions, a linearly declining neutron-separation energy with mass number for an isotopic chain gives a Gaussian equilibrium abundance distribution. The location of the peak of the Gaussian is essentially the mass number at which the neutron-separation energy is equal to the negative of the free neutron chemical potential less the neutron rest mass. The width of the Gaussian is given by the square root of the ratio of  $kT/S_1$ , the energy corresponding to the equilibrium temperature, divided by the magnitude of the slope of the neutron-separation energy curve. A lower temperature of the r-process environment or a steeper slope of the

neutron-separation energy curve gives a narrower abundance distribution.

We studied the equilibrium isotopic abundance curves from other neutron-separation energy curves with isotope mass number. We found that all effects could be interpreted in terms of modifications to the original linearly declining neutron-separation energy curve with mass number through the addition of spikes of varying magnitude at particular mass numbers. The result for the abundance curve was to transfer the abundance from one Gaussian to another for each spike encountered. This result allows one to infer the effects of any type of variation in nuclear masses or neutron-separation energies on resulting equilibrium distributions. We then pointed out that our analysis applies equally well to the  $(p, \gamma) - (\gamma, p)$  equilibrium that can occur in some proton-rich astrophysical environments.

In matter expansions relevant for r-process nucleosynthesis, the reaction network eventually falls out of  $(n, \gamma) - (\gamma, n)$  equilibrium. This occurs as the number of free neutrons falls below the number of nuclei. In this r-process freezeout, reactions occur that shuffle neutrons among the nuclei and shape the final abundance curve. Our next step is to follow that complex phase. The knowledge developed in the present work regarding  $(n, \gamma) - (\gamma, n)$  equilibrium will be essential for that work since it will delineate the starting point for freezeout. Also, since the freezeout reactions still strive to drive the abundances towards equilibrium, this knowledge will clarify the reaction network's goal during freezeout, no matter how unattainable.

## Appendix A: Confirmation of Eq. (41)

Since the finite integral in Eq. (32) is linear in its integrand, we may write

$$\left[ \int_{x_0}^x (x' - x_0)^p dx' \right]^+ = \sum_{n=0}^p \binom{p}{n} (-x_0)^{p-n} \left[ \int_{x_0}^x x'^n dx' \right]^+ \quad (\text{A1})$$

for non-negative integer  $p$ . From Eq. (40), we then find

$$\left[ \int_{x_0}^x (x' - x_0)^p dx' \right]^+ = \sum_{n=0}^p \binom{p}{n} (-x_0)^{p-n} \left[ \frac{B_{n+1}(x+1) - B_{n+1}(x_0+1)}{n+1} \right] \quad (\text{A2})$$

With the substitution  $m = n + 1$ , this may be written

$$\left[ \int_{x_0}^x (x' - x_0)^p dx' \right]^+ = \frac{1}{p+1} \sum_{m=0}^{p+1} \binom{p+1}{m} (-x_0)^{p+1-m} [B_m(x+1) - B_m(x_0+1)] \quad (\text{A3})$$

The lower limit  $m = 0$  holds because  $B_0(x) = 1$  so the  $m = 0$  term does not in fact contribute to the sum which may thus be extended from the  $m = 1$  limit arising from the  $m = n + 1$  substitution. From the property of Bernoulli polynomials that

$$B_n(x+y) = \sum_{k=0}^n \binom{n}{k} B_k(x) y^{n-k} \quad (\text{A4})$$

we then find

$$\left[ \int_{x_0}^x (x' - x_0)^p dx' \right]^+ = \frac{1}{p+1} [B_{p+1}(x - x_0 + 1) - B_{p+1}(1)] \quad (\text{A5})$$

This explicitly confirms Eq. (41). The integral in Eq. (42) may be confirmed similarly.

## Appendix B: Integer polynomials of inverse argument

We consider integer functions with  $F(x) = x^{-p}$ , where  $p$  is an integer and  $p > 0$  for  $x > 1$ . The backward derivative is

$$\left[ \frac{\partial}{\partial x} x^{-p} \right]_y^- = x^{-p} - x^{-p} (1 - x^{-1})^{-p} = - \sum_{k=1}^{\infty} \binom{p+k-1}{k} x^{-p-k} \quad (\text{B1})$$

Similarly, the forward derivative is

$$\left[ \frac{\partial}{\partial x} x^{-p} \right]_y^+ = x^{-p} (1 + x^{-1})^{-p} - x^{-p} = \sum_{k=1}^{\infty} (-1)^k \binom{p+k-1}{k} x^{-p-k} \quad (\text{B2})$$

In either case, the leading term is  $-px^{-p-1}$ , as expected.

The negative integral is

$$\left[ \int_{x_0}^x (x')^{-p} dx' \right]^- = \sum_{x'=x_0}^{x-1} x'^{-p} = \sum_{x'=1}^{x-1} x'^{-p} - \sum_{x'=1}^{x_0-1} x'^{-p} \quad (\text{B3})$$

This may be written

$$\left[ \int_{x_0}^x (x')^{-p} dx' \right]^- = H_{x-1,p} - H_{x_0-1,p} \quad (\text{B4})$$

where  $H_{x,p}$  is the generalized harmonic number given by

$$H_{x,p} = \sum_{k=1}^x \frac{1}{k^p} \quad (\text{B5})$$

Similarly,

$$\left[ \int_{x_0}^x (x')^{-p} dx' \right]^+ = H_{x,p} - H_{x_0,p} \quad (\text{B6})$$

We can check those integrals by taking their inverse derivatives

$$\left[ \frac{\partial}{\partial x} \left[ \int_{x_0}^x (x')^{-p} dx' \right]^+ \right]_y^- = H_{x,p} - H_{x-1,p} = x^{-p} \quad (\text{B7})$$

$$\left[ \frac{\partial}{\partial x} \left[ \int_{x_0}^x (x')^{-p} dx' \right]^- \right]_y^+ = H_{(x-1)+1,p} - H_{x-1,p} = x^{-p} \quad (\text{B8})$$

which are the expected results.

### Appendix C: Derivation of Eq. (67)

From Eq. (62), we may use the binomial expansion to find

$$A_0(\tilde{Z})^{k-p} = C_1^{k-p} + \sum_{j=0}^{k-p-1} \binom{k-p}{j} C_1^j (C_2+1)^{k-p-j} \tilde{Z}^{k-p-j} \quad (\text{C1})$$

Similarly, from Eq. (63), we find

$$Z_0(A)^{k-p} - Z_0(A-1)^{k-p} = \frac{1}{(C_2+1)^{k-p}} \sum_{j=1}^{k-p} \binom{k-p}{j} (-1)^{j-1} \left[ (C_1+1)^j - C_1^j \right] A^{k-p-j} \quad (\text{C2})$$

Finally, through the use of Eq. (39), we find

$$B_{p+1}(Z) - B_{p+1}(\tilde{Z}) = \sum_{m=1}^{p+1} B_{p+1-m} Z^m - \sum_{m=1}^{p+1} B_{p+1-m} \tilde{Z}^m \quad (\text{C3})$$

With these results, Eq. (66) becomes

$$\begin{aligned}
S_n(Z, A) &= S_0 + \sum_{k=1}^{k_m} S_k \sum_{p=0}^k (-1)^p \binom{k}{p} C_1^{k-p} A^p \\
&+ \sum_{k=1}^{k_m} S_k \sum_{p=0}^k (-1)^p \binom{k}{p} A^p \sum_{j=0}^{k-p-1} \binom{k-p}{j} C_1^j (C_2 + 1)^{k-p-j} \tilde{Z}^{k-p-j} \\
&+ \sum_{k=1}^{k_m} Q_k \sum_{p=0}^{k-1} (-1)^p \binom{k}{p} \frac{1}{(C_2 + 1)^{k-p}} \sum_{j=1}^{k-p} \binom{k-p}{j} (-1)^{j-1} [(C_1 + 1)^j - C_1^j] A^{k-p-j} \\
&\frac{1}{p+1} \sum_{m=1}^{p+1} \binom{p+1}{m} B_{p+1-m} (Z^m - \tilde{Z}^m)
\end{aligned} \tag{C4}$$

The neutron-separation energy is the difference between mass excesses and should therefore not be dependent on the choice of  $\tilde{Z}$ . That this dependence should disappear results in the condition

$$\begin{aligned}
&\sum_{k=1}^{k_m} S_k \sum_{p=0}^{k-1} (-1)^p \binom{k}{p} A^p \sum_{j=0}^{k-p-1} \binom{k-p}{j} C_1^j (C_2 + 1)^{k-p-j} \tilde{Z}^{k-p-j} \\
&= \sum_{k=1}^{k_m} Q_k \sum_{p=0}^{k-1} (-1)^p \binom{k}{p} \frac{1}{(C_2 + 1)^{k-p}} \sum_{j=1}^{k-p} \binom{k-p}{j} (-1)^{j-1} [(C_1 + 1)^j - C_1^j] A^{k-p-j} \quad (C5) \\
&\frac{1}{p+1} \sum_{m=1}^{p+1} \binom{p+1}{m} B_{p+1-m} \tilde{Z}^m
\end{aligned}$$

We begin analyzing this equation by noting that, with the substitution  $\ell = k - j$ , the left-hand side (LHS) of Eq. (C5) may be written

$$LHS = \sum_{k=1}^{k_m} S_k \sum_{p=0}^{k-1} \sum_{\ell=p+1}^k (-1)^p \binom{k}{p} \binom{k-p}{k-\ell} C_1^{k-\ell} (C_2 + 1)^{\ell-p} A^p \tilde{Z}^{\ell-p} \tag{C6}$$

We now exchange the sums on  $p$  and  $\ell$  to find

$$LHS = \sum_{k=1}^{k_m} S_k \sum_{\ell=1}^k \binom{k}{k-\ell} C_1^{k-\ell} (C_2 + 1)^\ell \sum_{p=0}^{\ell-1} (-1)^p \binom{\ell}{p} (C_2 + 1)^{-p} A^p \tilde{Z}^{\ell-p} \tag{C7}$$

We write this as

$$LHS = \sum_{k=1}^{k_m} S_k \sum_{\ell=1}^k \alpha_\ell^{(k)} \tilde{Z}^\ell \tag{C8}$$

where

$$\alpha_\ell^{(k)} = \binom{k}{k-\ell} C_1^{k-\ell} (C_2 + 1)^\ell \tag{C9}$$

and

$$\tilde{Z}^\ell = \sum_{p=0}^{\ell-1} (-1)^p \binom{\ell}{p} (C_2 + 1)^{-p} A^p \tilde{Z}^{\ell-p} \quad (\text{C10})$$

Upon exchange of the sums on  $p$  and  $j$ , the right-hand side (RHS) of Eq. (C5) becomes

$$RHS = \sum_{k=1}^{k_m} Q_k \sum_{j=1}^k \sum_{p=0}^{k-j} \sum_{m=1}^{p+1} (-1)^p \binom{k}{p} \binom{k-p}{j} \binom{p+1}{m} \frac{(-1)^{j-1} [(C_1+1)^j - C_1^j]}{(C_2+1)^{k-p}} \frac{B_{p+1-m}}{p+1} \tilde{Z}^m A^{k-p-j} \quad (\text{C11})$$

We now exchange the sums on  $p$  and  $m$  and simplify terms to get

$$RHS = \sum_{k=1}^{k_m} Q_k \sum_{j=1}^k \sum_{m=1}^{k-j+1} \sum_{p=m-1}^{k-j} (-1)^{p+j-1} \frac{k!}{(k-p-j)!j!(p+1-m)!m!} \frac{[(C_1+1)^j - C_1^j]}{(C_2+1)^{k-p}} B_{p+1-m} \tilde{Z}^m A^{k-p-j} \quad (\text{C12})$$

We make the substitution  $\ell = m + k - p - j$  to find

$$RHS = \sum_{k=1}^{k_m} Q_k \sum_{j=1}^k \sum_{m=1}^{k-j+1} \sum_{\ell=m}^{k-j+1} (-1)^{m+k-\ell-1} \frac{k!}{(\ell-m)!j!(k-\ell-j+1)!m!} \frac{[(C_1+1)^j - C_1^j]}{(C_2+1)^{\ell-m+j}} B_{k-\ell-j+1} \tilde{Z}^m A^{\ell-m} \quad (\text{C13})$$

We now exchange the  $m$  and  $\ell$  and then  $j$  and  $\ell$  sums to get

$$RHS = \sum_{k=1}^{k_m} Q_k (-1)^{k-1} \sum_{\ell=1}^k (-1)^\ell \frac{k!}{\ell!} (C_2 + 1)^{-\ell} \sum_{m=1}^{\ell} (-1)^m \binom{\ell}{m} (C_2 + 1)^m \tilde{Z}^m A^{\ell-m} \quad (\text{C14})$$

$$\sum_{j=1}^{k-\ell+1} \frac{[(C_1+1)^j - C_1^j]}{(k-\ell-j+1)!j!(C_2+1)^j} B_{k-\ell-j+1}$$

Finally, with the replacement  $q = \ell - m$  we find

$$RHS = \sum_{k=1}^{k_m} Q_k (-1)^{k-1} \sum_{\ell=1}^k \frac{k!}{\ell!} \sum_{q=0}^{\ell-1} (-1)^q \binom{\ell}{q} (C_2 + 1)^{-q} \tilde{Z}^{\ell-q} A^q \quad (\text{C15})$$

$$\sum_{j=1}^{k-\ell+1} \frac{[(C_1+1)^j - C_1^j]}{(k-\ell-j+1)!j!(C_2+1)^j} B_{k-\ell-j+1}$$

With Eq. (C10), this becomes

$$RHS = \sum_{k=1}^{k_m} Q_k \sum_{\ell=1}^k \beta_\ell^{(k)} \tilde{Z}^\ell \quad (\text{C16})$$

with

$$\beta_\ell^{(k)} = (-1)^{k-1} \frac{k!}{\ell!} \sum_{j=1}^{k-\ell+1} \frac{[(C_1+1)^j - C_1^j]}{(k-\ell-j+1)!j!(C_2+1)^j} B_{k-\ell-j+1} \quad (\text{C17})$$

From Eqs. (C8) and (C16), Eq. (C5) becomes

$$\sum_{k=1}^{k_m} S_k \sum_{\ell=1}^k \alpha_\ell^{(k)} \tilde{Z}^{\ell} = \sum_{k=1}^{k_m} Q_k \sum_{\ell=1}^k \beta_\ell^{(k)} \tilde{Z}^{\ell} \quad (\text{C18})$$

If we exchange the sums on  $k$  and  $\ell$ , we then find

$$\sum_{\ell=1}^{k_m} \tilde{Z}^{\ell} \sum_{k=\ell}^{k_m} \alpha_\ell^{(k)} S_k = \sum_{\ell=1}^{k_m} \tilde{Z}^{\ell} \sum_{k=\ell}^{k_m} \beta_\ell^{(k)} Q_k \quad (\text{C19})$$

Equating equal powers of  $\tilde{Z}^{\ell}$  results in the equation

$$\sum_{k=\ell}^{k_m} \beta_\ell^{(k)} Q_k = \sum_{k=\ell}^{k_m} \alpha_\ell^{(k)} S_k \quad (\text{C20})$$

In specifying our nuclear model, we choose  $S_k$  for  $k = 0$  to  $k = k_m$ . If we choose  $\ell = k_m$  in Eq. (C20), we find

$$Q_{k_m} = \frac{\alpha_{k_m}^{(k_m)}}{\beta_{k_m}^{(k_m)}} S_{k_m} \quad (\text{C21})$$

Other values of  $Q_\ell$  may then be found from the previously determined values  $Q_k$  with  $k > \ell$  from

$$Q_\ell = \frac{1}{\beta_\ell^{(\ell)}} \left[ \sum_{k=\ell}^{k_m} \alpha_\ell^{(k)} S_k - \sum_{k=\ell+1}^{k_m} \beta_\ell^{(k)} Q_k \right] \quad (\text{C22})$$

## Acknowledgments

This work was supported by NASA grant 80NSSC20K0338. The authors thank Yuko Motizuki and Jared Friedl for valuable discussions.

- 
- [1] E. M. Burbidge, G. R. Burbidge, W. A. Fowler, and F. Hoyle, *Reviews of Modern Physics* **29**, 547 (1957).
  - [2] W. Hillebrandt, K. Takahashi, and T. Kodama, *Astron. Ap.* **52**, 63 (1976).
  - [3] S. E. Woosley, J. R. Wilson, G. J. Mathews, R. D. Hoffman, and B. S. Meyer, *Astrophys. J.* **433**, 229 (1994).
  - [4] T. Fischer, M.-R. Wu, B. Wehmeyer, N.-U. F. Bastian, G. Martínez-Pinedo, and F.-K. Thielemann, *The Astrophysical Journal* **894**, 9 (2020), URL <https://doi.org/10.3847/1538-4357/ab86b0>.

- [5] J. M. Lattimer, F. Mackie, D. G. Ravenhall, and D. N. Schramm, *Astrophys. J.* **213**, 225 (1977).
- [6] B. S. Meyer, *Astrophys. J.* **343**, 254 (1989).
- [7] D. Eichler, M. Livio, T. Piran, and D. N. Schramm, *Nature (London)* **340**, 126 (1989).
- [8] D. M. Siegel, J. Barnes, and B. D. Metzger, *Nature (London)* **569**, 241 (2019), 1810.00098.
- [9] B. P. Abbott, R. Abbott, T. D. Abbott, F. Acernese, K. Ackley, C. Adams, T. Adams, P. Addesso, R. X. Adhikari, V. B. Adya, et al., *Phys. Rev. Lett.* **119**, 161101 (2017), 1710.05832.
- [10] D. Kasen, B. Metzger, J. Barnes, E. Quataert, and E. Ramirez-Ruiz, *Nature (London)* **551**, 80 (2017), 1710.05463.
- [11] B. D. Metzger, G. Martínez-Pinedo, S. Darbha, E. Quataert, A. Arcones, D. Kasen, R. Thomas, P. Nugent, I. V. Panov, and N. T. Zinner, *Mon. Not. Royal Astr. Soc.* **406**, 2650 (2010), 1001.5029.
- [12] N. Nishimura, T. Takiwaki, and F.-K. Thielemann, *Astrophys. J.* **810**, 109 (2015), 1501.06567.
- [13] T. C. Beers and N. Christlieb, *Ann. Rev. Astron. Ap.* **43**, 531 (2005).
- [14] C. Kobayashi, A. I. Karakas, and M. Lugaro, *Astrophys. J.* **900**, 179 (2020), 2008.04660.
- [15] G. Lorusso, S. Nishimura, Z. Y. Xu, A. Jungclaus, Y. Shimizu, G. S. Simpson, P.-A. Söderström, H. Watanabe, F. Browne, P. Doornenbal, et al., *Physical Review Letters* **114**, 192501 (2015).
- [16] M. R. Mumpower, R. Surman, D. L. Fang, M. Beard, P. Möller, T. Kawano, and A. Aprahamian, *Phys. Rev. C* **92**, 035807 (2015), 1505.07789.
- [17] T. Kajino and G. J. Mathews, *Reports on Progress in Physics* **80**, 084901 (2017), 1610.07929.
- [18] B. S. Meyer and J. S. Brown, *Astrophys. J. Suppl.* **112**, 199 (1997).
- [19] D. Martin, A. Arcones, W. Nazarewicz, and E. Olsen, *Phys. Rev. Lett.* **116**, 121101 (2016), URL <https://link.aps.org/doi/10.1103/PhysRevLett.116.121101>.
- [20] B. Zhao and S. Q. Zhang, *The Astrophysical Journal* **874**, 5 (2019), URL <https://doi.org/10.3847/1538-4357/ab0702>.
- [21] B. Sun, F. Montes, L. S. Geng, H. Geissel, Y. A. Litvinov, and J. Meng, *Phys. Rev. C* **78**, 025806 (2008), 0710.2332.
- [22] K. Farouqi, K. L. Kratz, B. Pfeiffer, T. Rauscher, F. K. Thielemann, and J. W. Truran, *Astrophys. J.* **712**, 1359 (2010), 1002.2346.
- [23] R. Surman, J. Engel, J. R. Bennett, and B. S. Meyer, *Phys. Rev. Lett.* **79**, 1809 (1997), URL

- <https://link.aps.org/doi/10.1103/PhysRevLett.79.1809>.
- [24] M. Mumpower, R. Surman, G. McLaughlin, and A. Aprahamian, *Progress in Particle and Nuclear Physics* **86**, 86 (2016), ISSN 0146-6410, URL <https://www.sciencedirect.com/science/article/pii/S0146641015000897>.
- [25] P. A. Seeger, W. A. Fowler, and D. D. Clayton, *Astrophys. J. Suppl.* **11**, 121 (1965).
- [26] K.-L. Kratz, J.-P. Bitouzet, F.-K. Thielemann, P. Moeller, and B. Pfeiffer, *Astrophys. J.* **403**, 216 (1993).
- [27] K. L. Kratz, B. Pfeiffer, and F. K. Thielemann, *Nucl. Phys. A* **630**, 352 (1998).
- [28] <https://github.com/mengkel/ng-gn-abundances>; see also <http://webnucleo.org>.
- [29] B. S. Meyer, T. D. Krishnan, and D. D. Clayton, *Astrophys. J.* **498**, 808 (1998).
- [30] B. S. Meyer, G. C. McLaughlin, and G. M. Fuller, *Phys. Rev. C* **58**, 3696 (1998).
- [31] B. S. Meyer, T. D. Krishnan, and D. D. Clayton, *Astrophys. J.* **462**, 825 (1996).
- [32] B. S. Meyer, *NucNet Tools*, <https://sourceforge.net/p/nucnet-tools/home/Home/>.
- [33] C. F. V. Weizsäcker, *Zeitschrift für Physik* **96**, 431 (1935).
- [34] B. Taylor, *Methodus incrementorum directa & inversa* (William Innys, London, 1715).
- [35] R. H. Cyburt, A. M. Amthor, R. Ferguson, Z. Meisel, K. Smith, S. Warren, A. Heger, R. D. Hoffman, T. Rauscher, A. Sakharuk, et al., *Astrophys. J. Suppl.* **189**, 240 (2010).
- [36] J. W. Rohlf, *Modern Physics from  $\alpha$  to Z0* (1994).
- [37] B. S. Meyer, G. J. Mathews, W. M. Howard, S. E. Woosley, and R. D. Hoffman, *Astrophys. J.* **399**, 656 (1992).
- [38] C. Fröhlich, *Journal of Physics: Conference Series* **403**, 012034 (2012), URL <https://doi.org/10.1088/1742-6596/403/1/012034>.
- [39] C. Fröhlich, G. Martínez-Pinedo, M. Liebendörfer, F. K. Thielemann, E. Bravo, W. R. Hix, K. Langanke, and N. T. Zinner, *Phys. Rev. Lett.* **96**, 142502 (2006), [astro-ph/0511376](https://arxiv.org/abs/astro-ph/0511376).

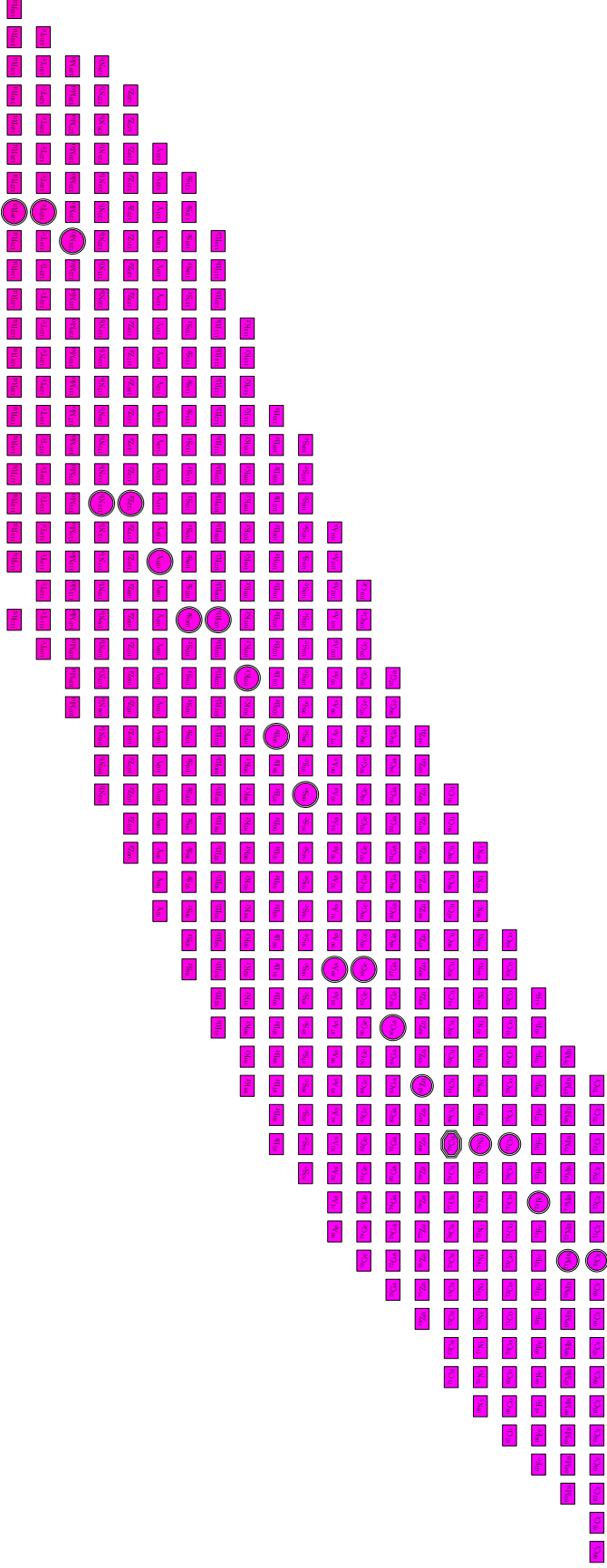


FIG. 1: (Color online) Chemical potential offset differences for the reference r-process calculation at the time step  $t = 0.243$  s,  $T_9 = 4.44$ , and mass density  $\rho = 8.78 \times 10^7$  g/cc. The chemical potential offset difference is the chemical potential offset relative to that for the maximum abundance species within the scope of the diagram (nuclides from Cr,  $Z = 24$ , to Ru,  $Z = 44$ ); thus, the quantity shown is  $\tilde{\mu}(Z, A)/kT - \tilde{\mu}(Z_{max}, A_{max})/kT$ , where  $Z_{max}$  and  $A_{max}$  are the atomic number and mass number of the maximum abundance species, respectively. The maximum abundance species within the scope of the diagram is indicated by the triple-outline octagon, while the maximum abundance species for other elements is indicated by the double-outlined circle. The color indicates the value chemical potential offset difference, and the value for any species may be inferred from Fig. 4. The chemical potential offset difference is only shown for species with abundance greater than  $10^{25}$  per nucleon.

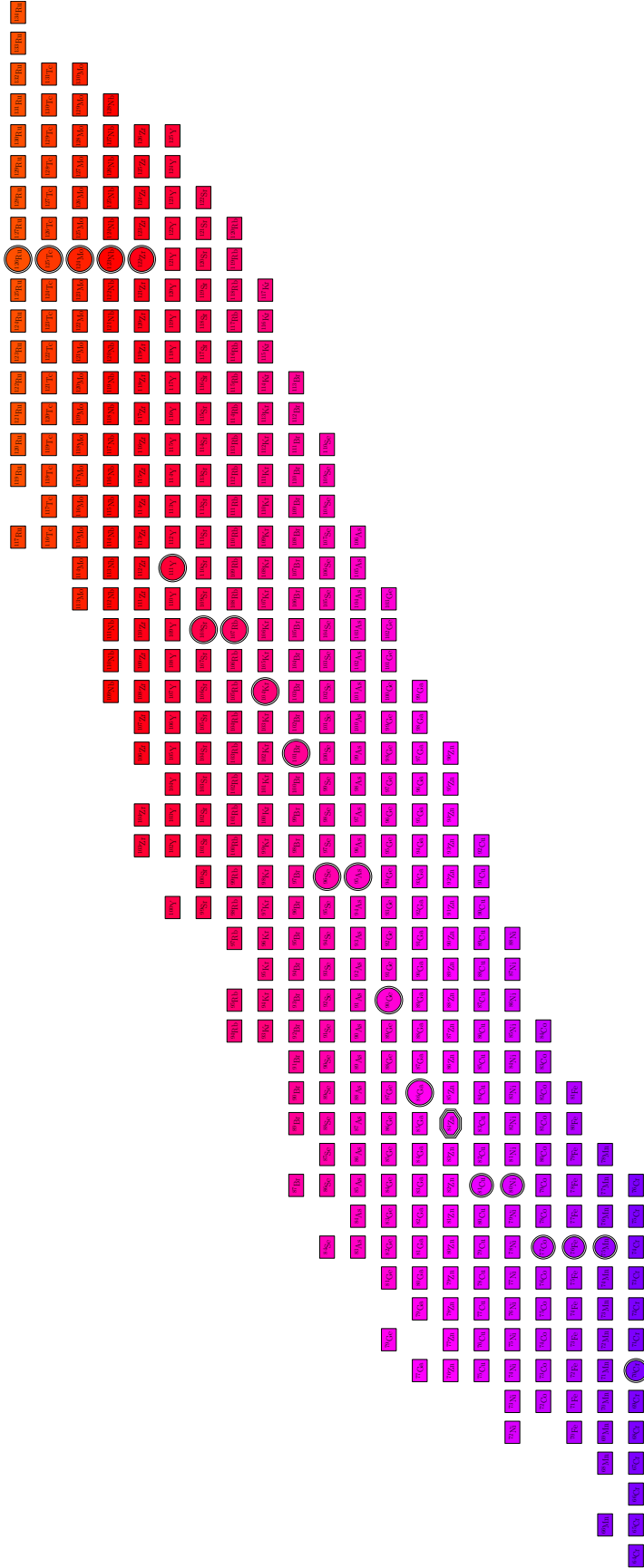


FIG. 2: (Color online) The same as Fig. 1 but for the time step  $0.332$  s,  $T_9 = 3.30$ , and  $\rho = 3.60 \times 10^7$  g/cc.

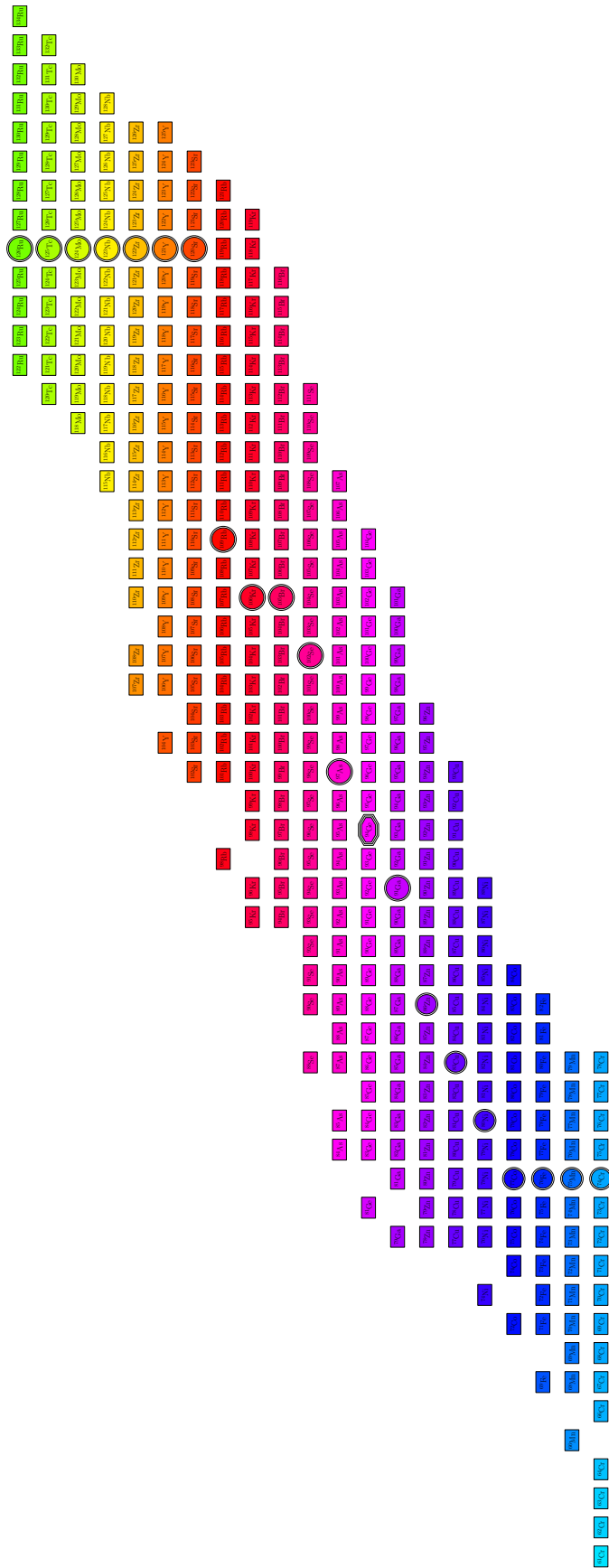


FIG. 3: (Color online) The same as Fig. 1 but for the time step  $0.432 \text{ s}$ ,  $T_9 = 2.369$ , and  $\rho = 1.33 \times 10^7 \text{ g/cc}$ .



FIG. 4: (Color online) The color bar for the chemical potential offset differences in Figs. 1, 2, and 3. The number inside each box gives the offset difference divided by  $kT$  for the corresponding color.

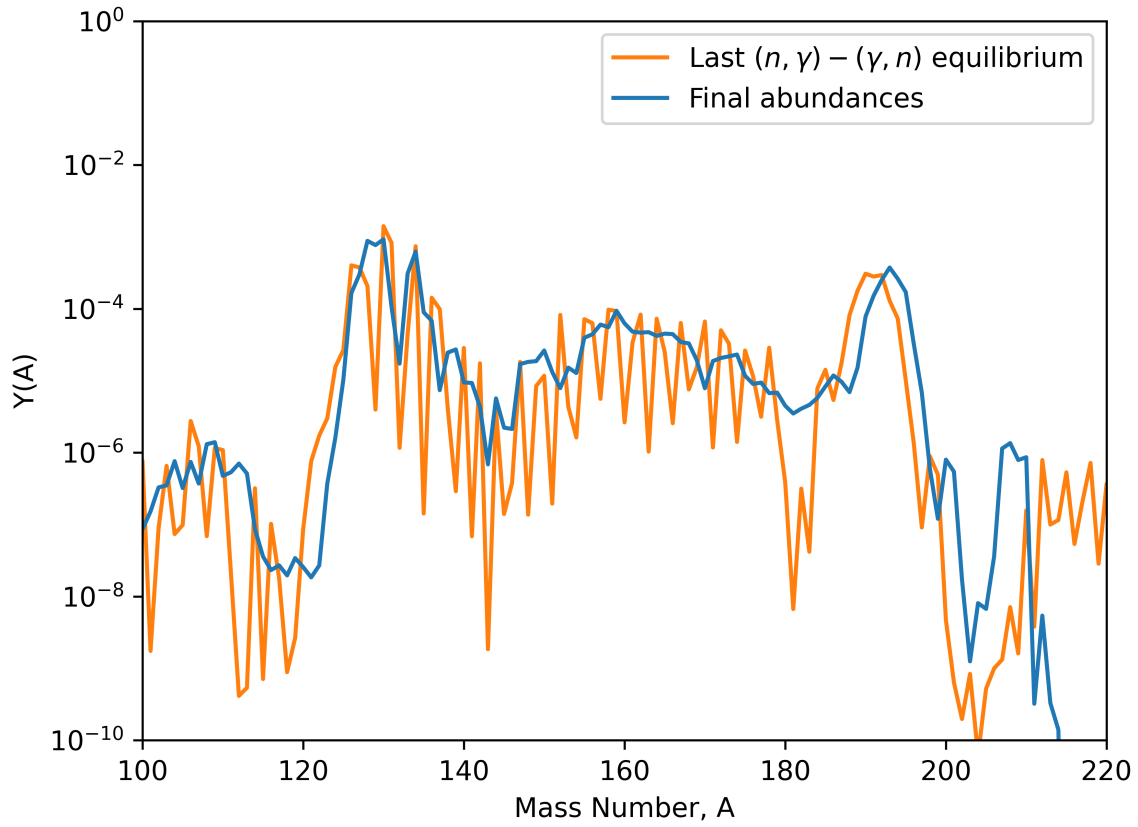


FIG. 5: (Color online) The abundances as a function of nucleon number for the last moment of  $(n, \gamma) - (\gamma, n)$  equilibrium and the final frozen-out abundances.

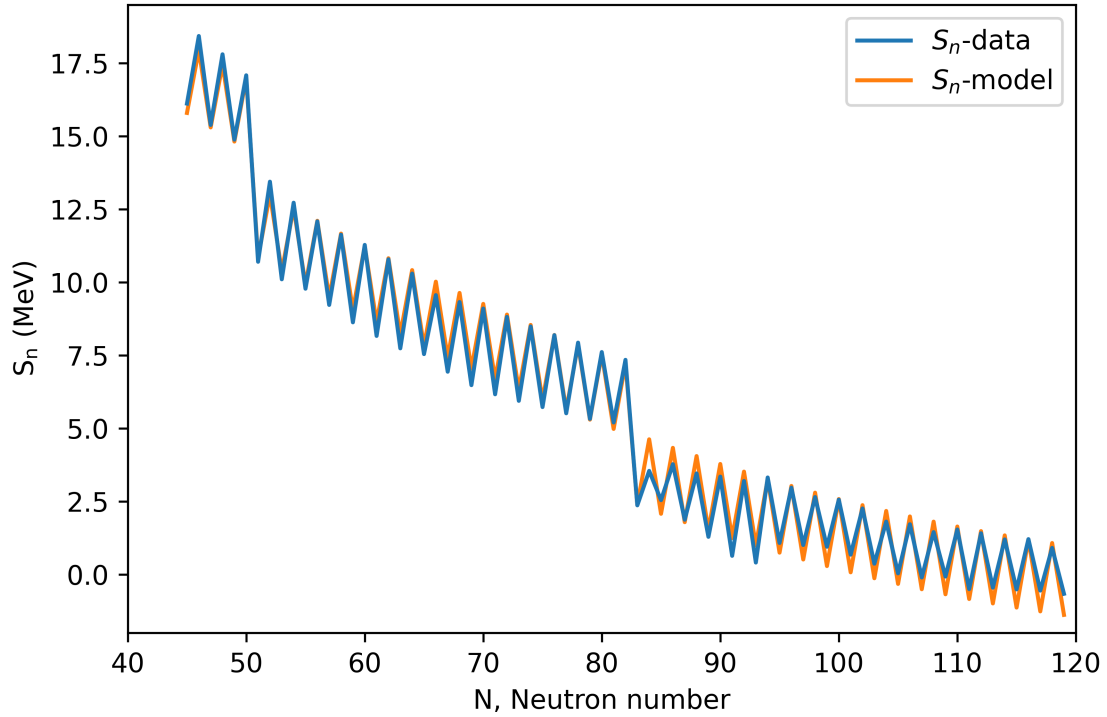


FIG. 6: (Color online) Neutron-separation energies as a function of neutron number  $N = A - Z$  for  $Z = 50$  from our model (orange line) and from those derived from the REACLIB V2.2 database [35] (blue line). The separation energies in our model were computed from Eq. (73) with  $[S_0, S_1, S_2, \delta_n, C_s] = [17, 0.25, 0.001, 1.2, 3.5]$ .

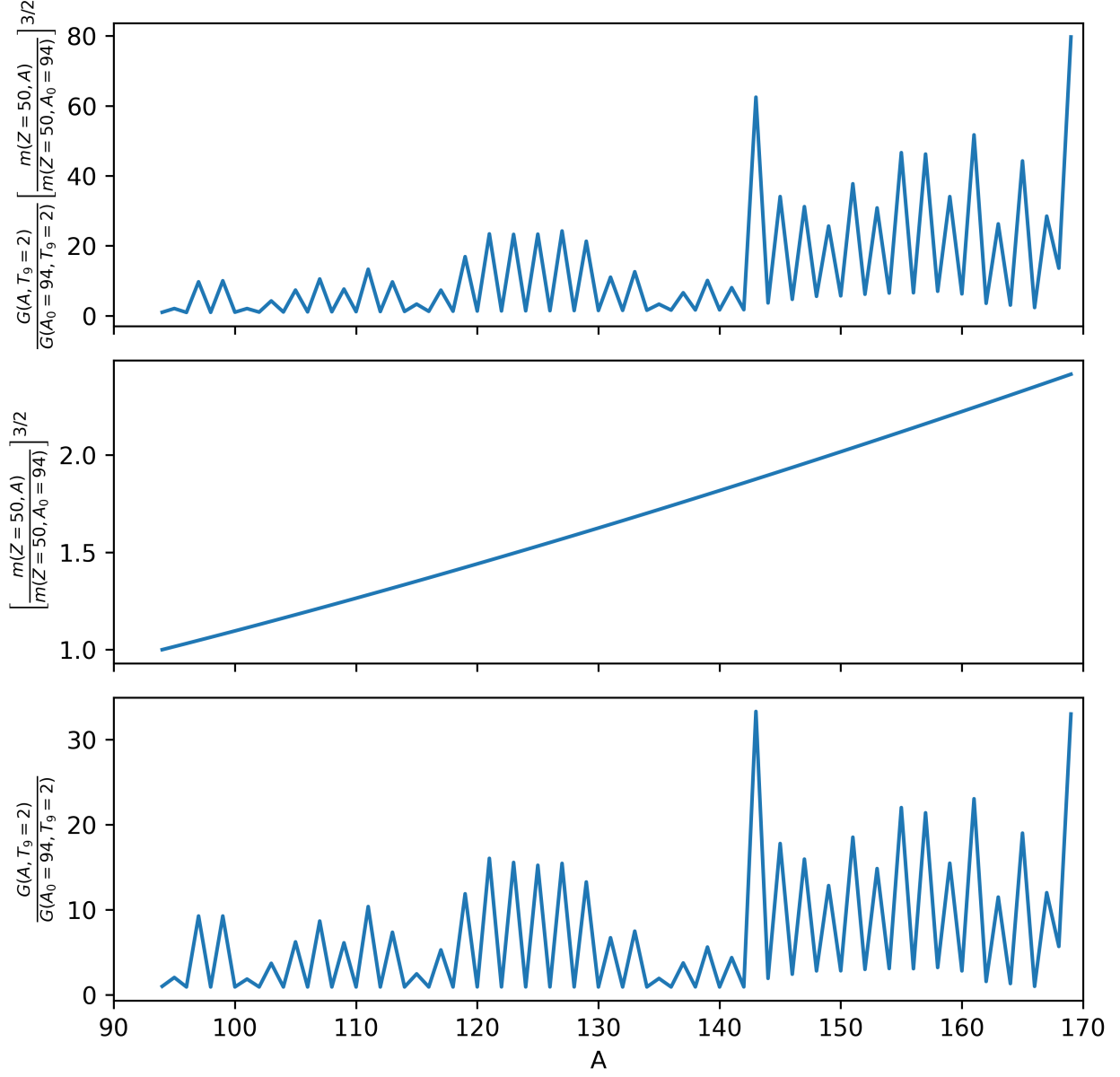


FIG. 7: (Color online) The upper panel shows the ratio values of  $G(Z, A)m(Z, A)^{3/2}$ ; The middle and lower panels show the ratio values of masses and partition functions, respectively, in an isotopic chain ( $Z = 50$ ). Data are from the REACLIB V2.2 database.

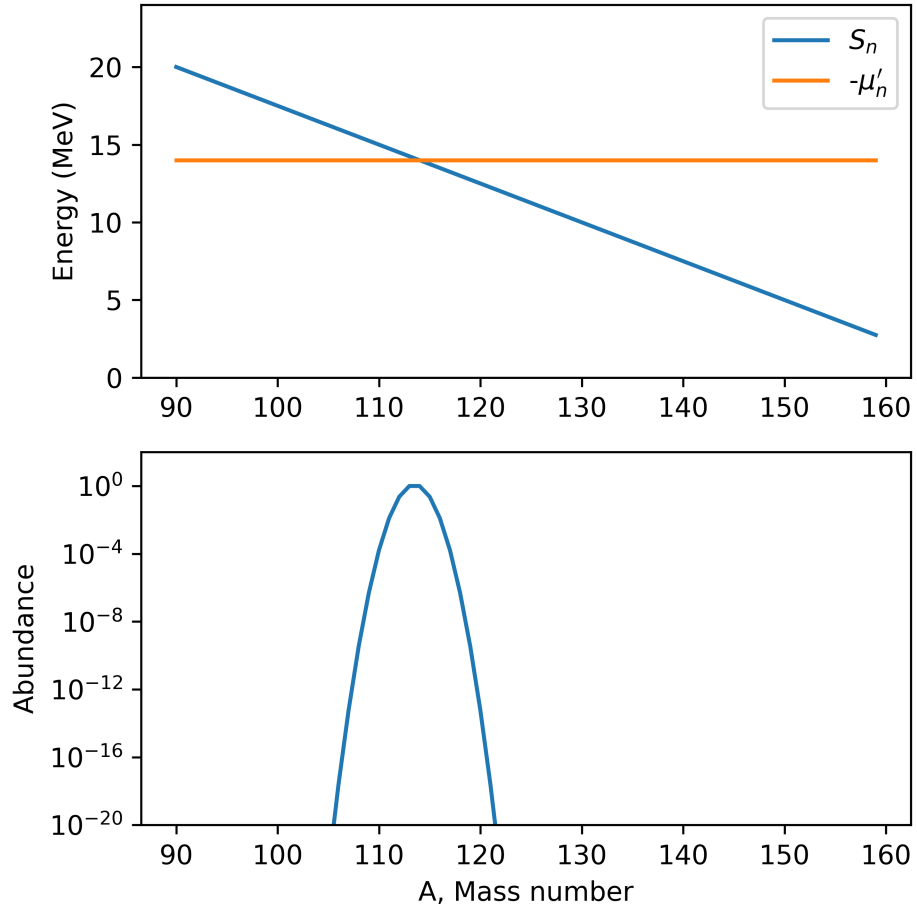


FIG. 8: (Color online) The upper panel shows the intersection of  $S_n$  and  $-\mu'_n$ . The lower panel presents the isotopic abundances within an isotope chain. The intersection position in the top panel is the abundance peak position in the lower panel

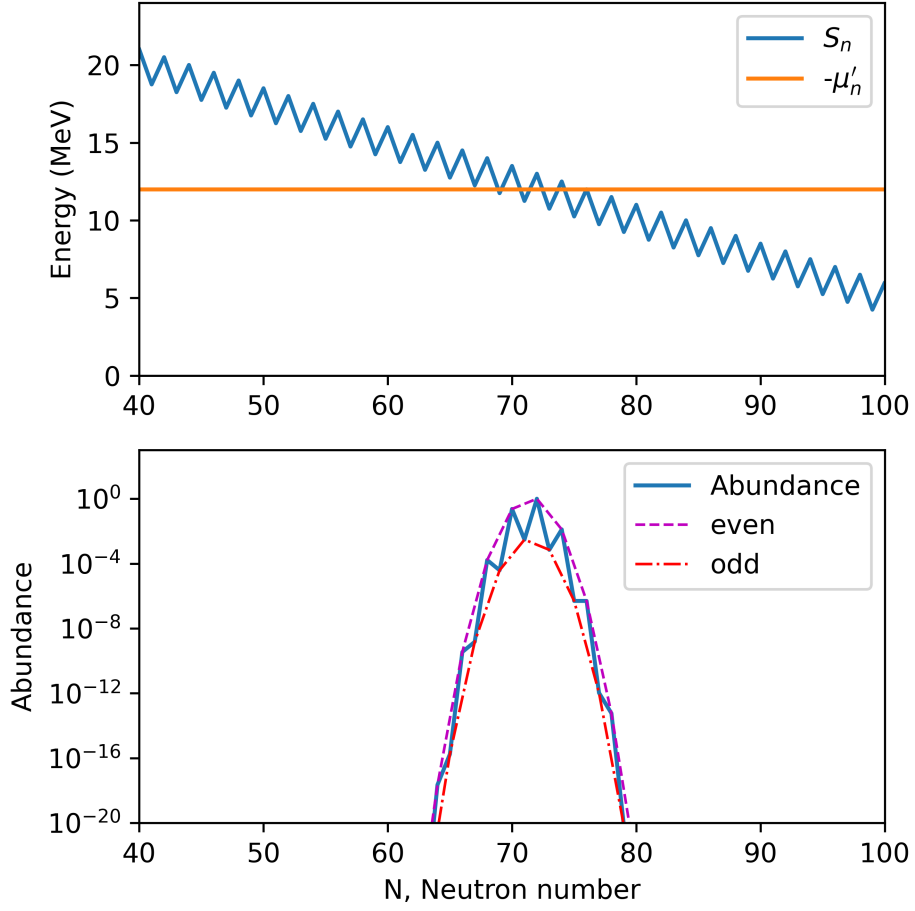


FIG. 9: (Color online) This figure shows the abundance distribution including both the linear and pairing term of  $S_n$ . The upper panel shows the intersection of  $S_n$  and  $-\mu'_n$ , while the solid line in the lower panel illustrates the abundance distribution. The dashed and dash-dotted lines are abundances curves, including purely even and odd  $N$ , respectively.

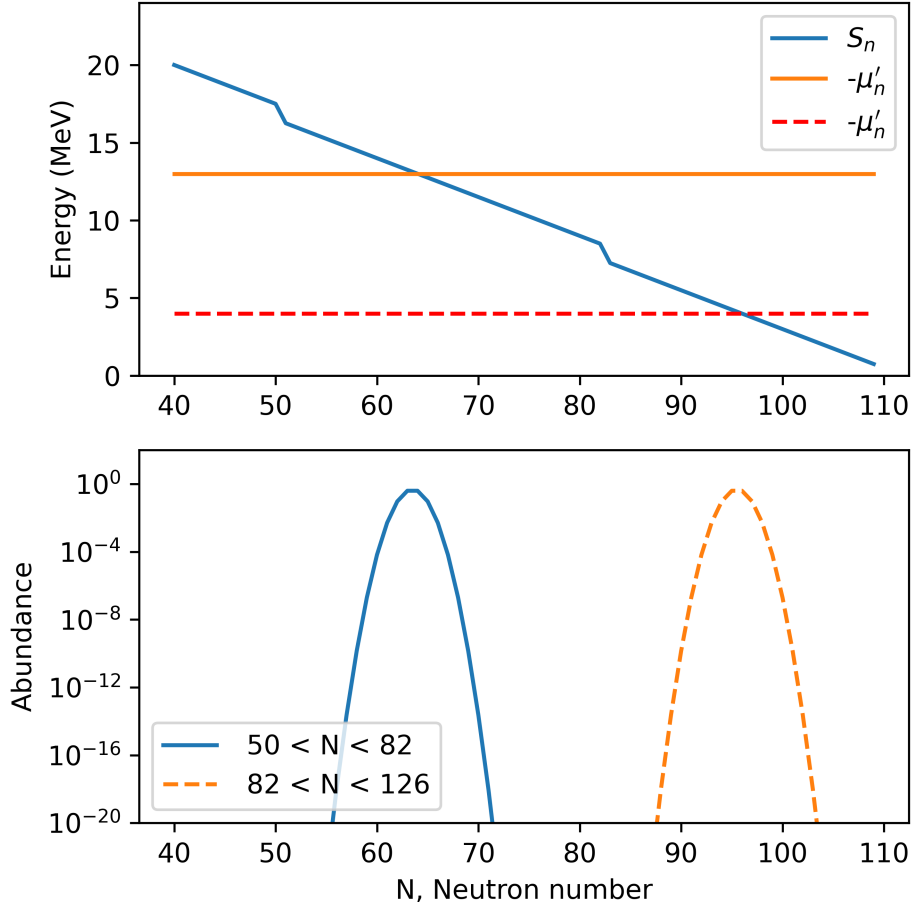
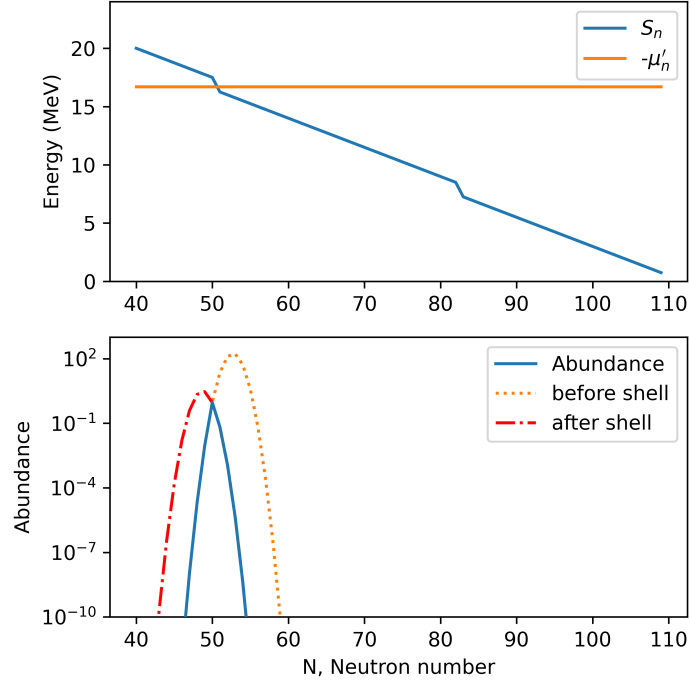
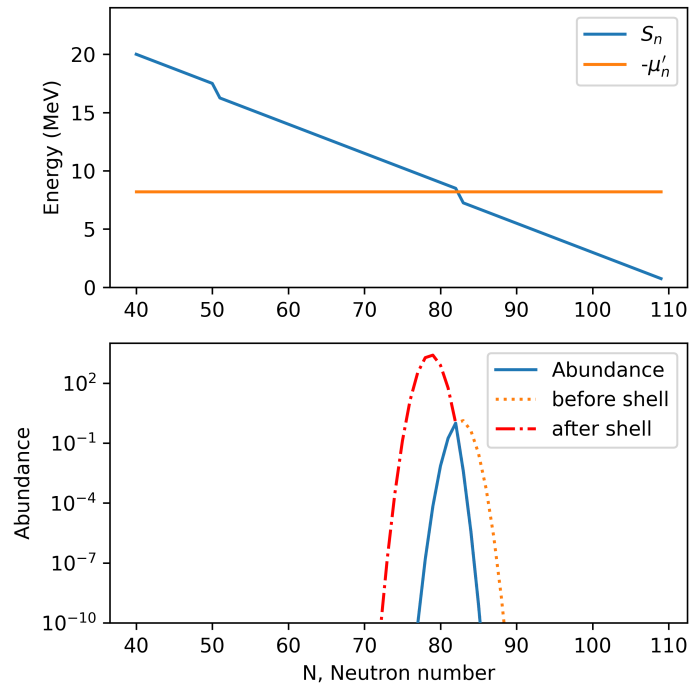


FIG. 10: (Color online) The upper panel shows the intersection of  $S_n$  and  $-\mu'_n$  at two different values of  $-\mu'_n$ . The intersections each occur at neutron numbers between two magic numbers. The lower panel presents the resulting equilibrium abundance distributions, which appear as full Gaussians since they do not cross any closed shell. This figure is using  $A_0 - Z = 40$ .



(a)  $N = 50$  Shell.



(b)  $N = 82$  Shell.

FIG. 11: (Color online) Results for (a) the  $N = 50$  shell crossing and (b) the  $N = 82$  shell crossing. The upper panel shows the intersection of relevant energies. The solid curve in the lower panel represents the full abundance distribution. The dash-dotted and dotted lines are Gaussian curves before and after a closed shell, respectively.

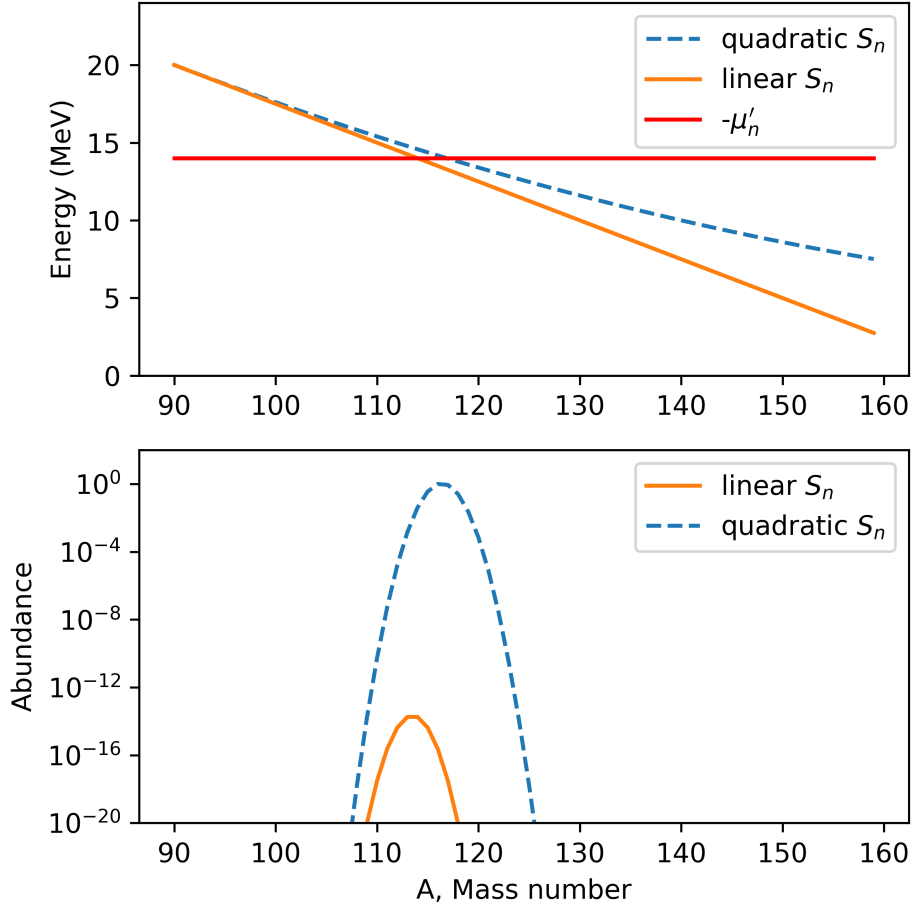


FIG. 12: (Color online) The upper panel shows the intersection of  $S_n$  and  $-\mu'_n$  for the case of the linear and quadratic  $S_n$ . The lower panel shows the resulting equilibrium abundance distributions. The distribution for the quadratic  $S_n$  is normalized, and the distribution for the linear  $S_n$  is computed from the same values of  $S_0$  and  $S_1$  as in the quadratic case. The quadratic term in  $S_n$  shifts the intersection to higher neutron number relative to that for the linear case. It also gives the resulting equilibrium abundance distribution a positive skew.

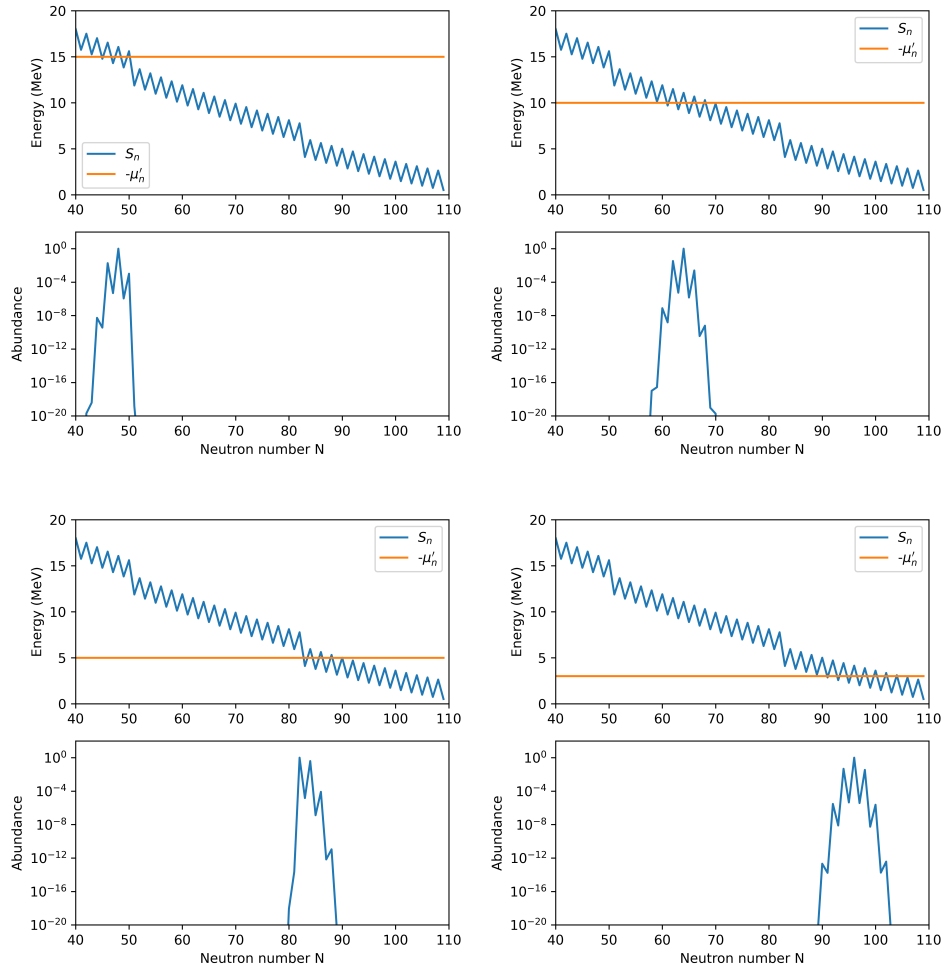
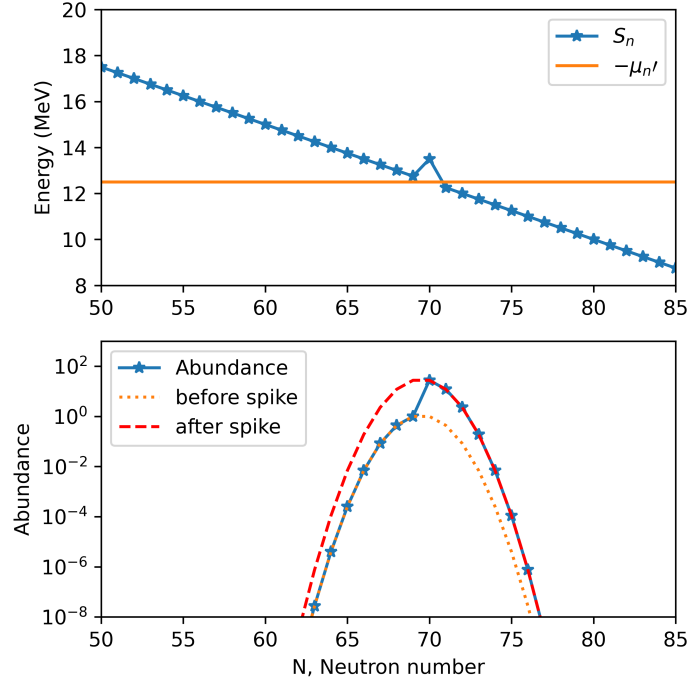
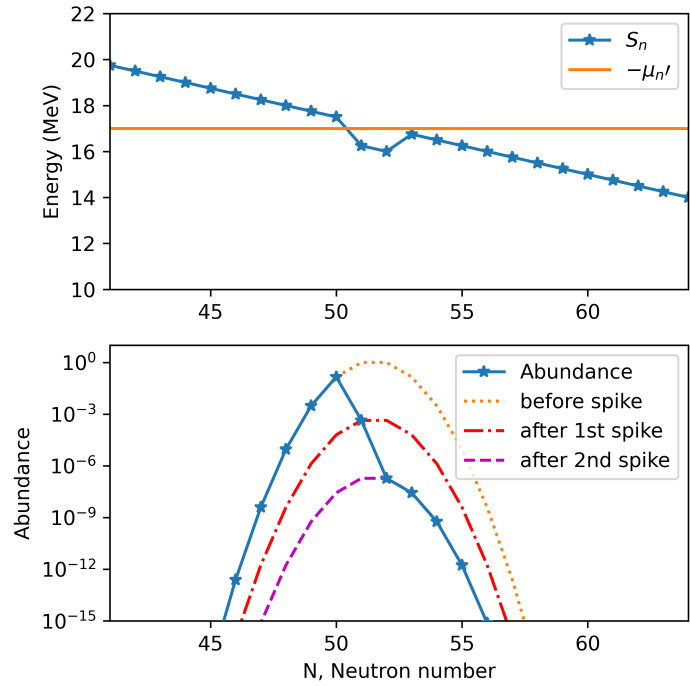


FIG. 13: (Color online) Each panel shows the intersection of  $S_n$  and  $\mu'_n$  in the upper part and the abundance distribution considering pairing and shell as well as quadratic terms in the lower part. From left to right, and top to bottom, we used  $-\mu'_n = 15, 10, 5, 3$  in each panel to demonstrate the abundance pattern.



(a) Single spike



(b) Two spikes

FIG. 14: (Color online) (a) The neutron-separation energy  $S_n$  with a single spike (upper panel) and the resulting equilibrium abundance curve. (b) The neutron-separation energy  $S_n$  with two successive negative spikes and the resulting equilibrium abundance curve.

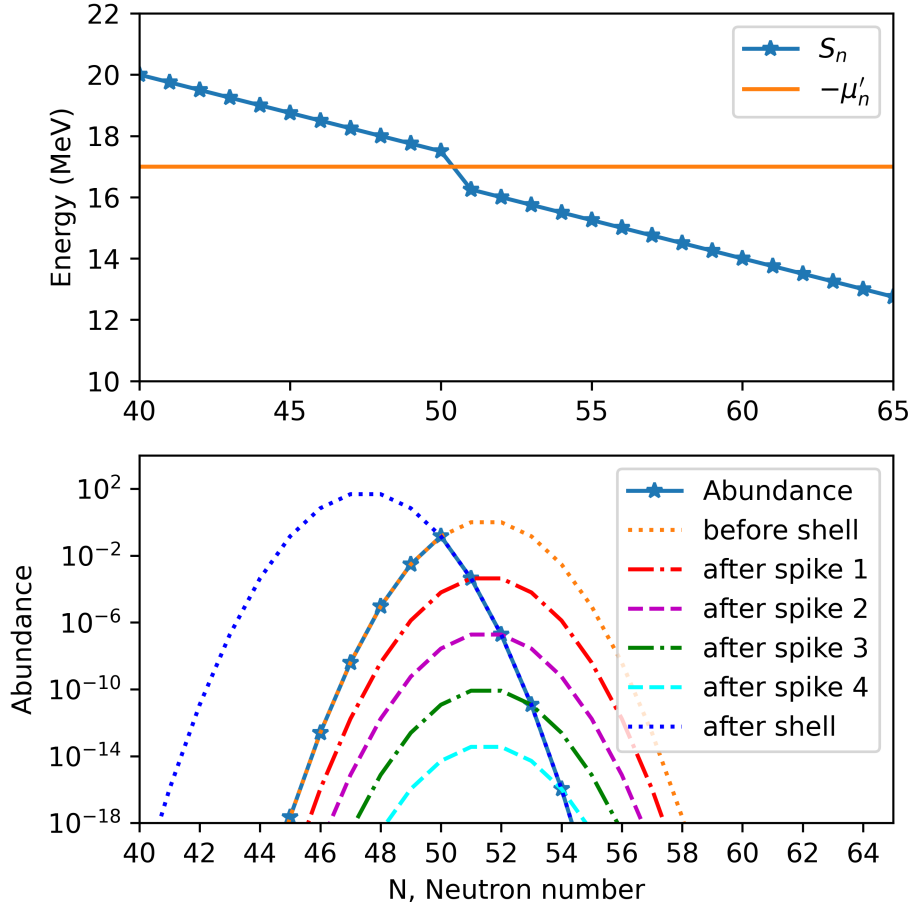


FIG. 15: (Color online) Neutron-separation for a single-shell transition. The shell effect may be considered a sequence of negative spikes added to the linearly declining separation energy. The lower panel shows the full abundance distribution. The abundance point after the neutron number corresponding to the first spike is on its own Gaussian distribution labeled in the legend. The resulting abundance distribution is a new Gaussian after the magic number.

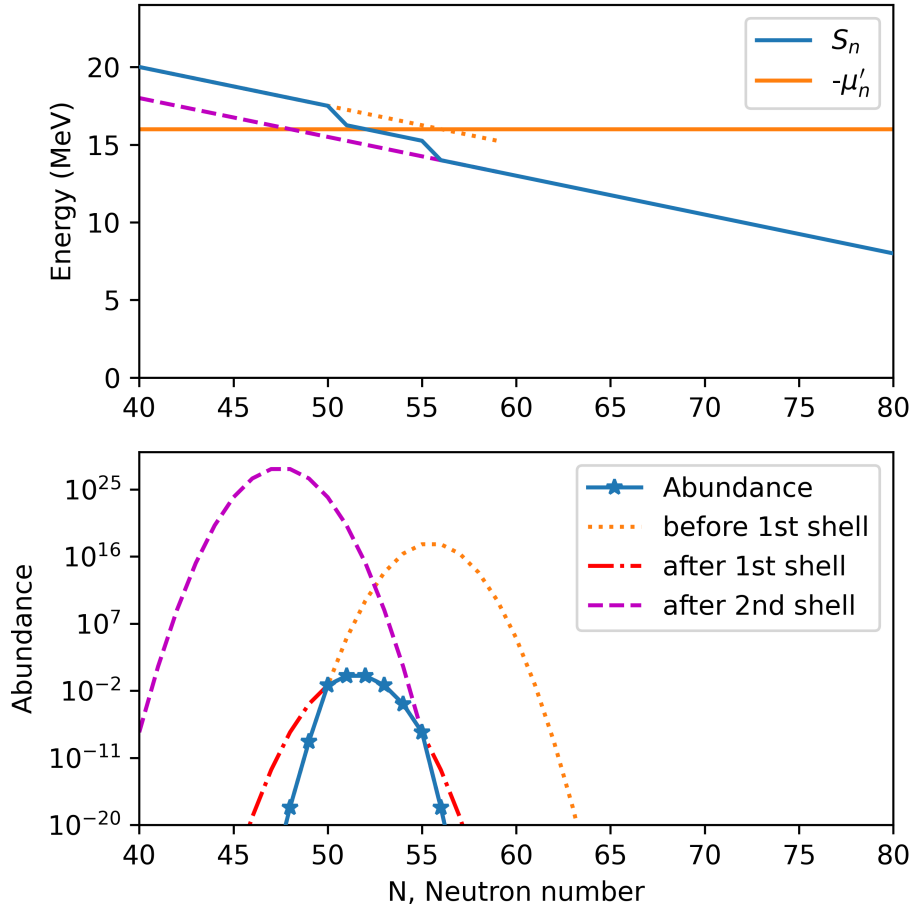


FIG. 16: (Color online) Neutron-separation for two shell transitions. As in Fig. 15, the shell effect may be considered a sequence of negative spikes added to the linearly declining separation energy. The second shell is then a second sequence of spikes added to the first. The lower panel shows the full abundance distribution and illustrates the transformation from one Gaussian to a second Gaussian after the first shell and then to a third Gaussian after the second shell.

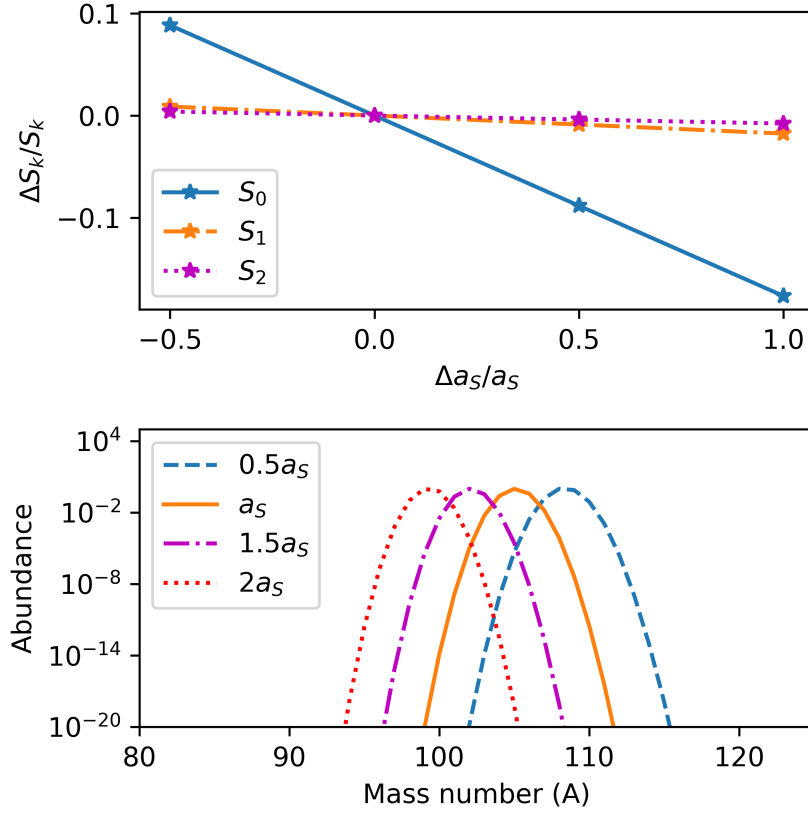


FIG. 17: (Color online) The upper panel shows the fractional change in  $S_0$ ,  $S_1$ , and  $S_2$  with the given variation in  $a_S$ , the surface-term coefficient in the liquid-drop model of Eq. (15). The lower panel shows the normalized equilibrium abundance curves resulting from the indicated variations in the surface term coefficient away from the reference value  $a_S$  for a fixed  $-\mu'_n$ .

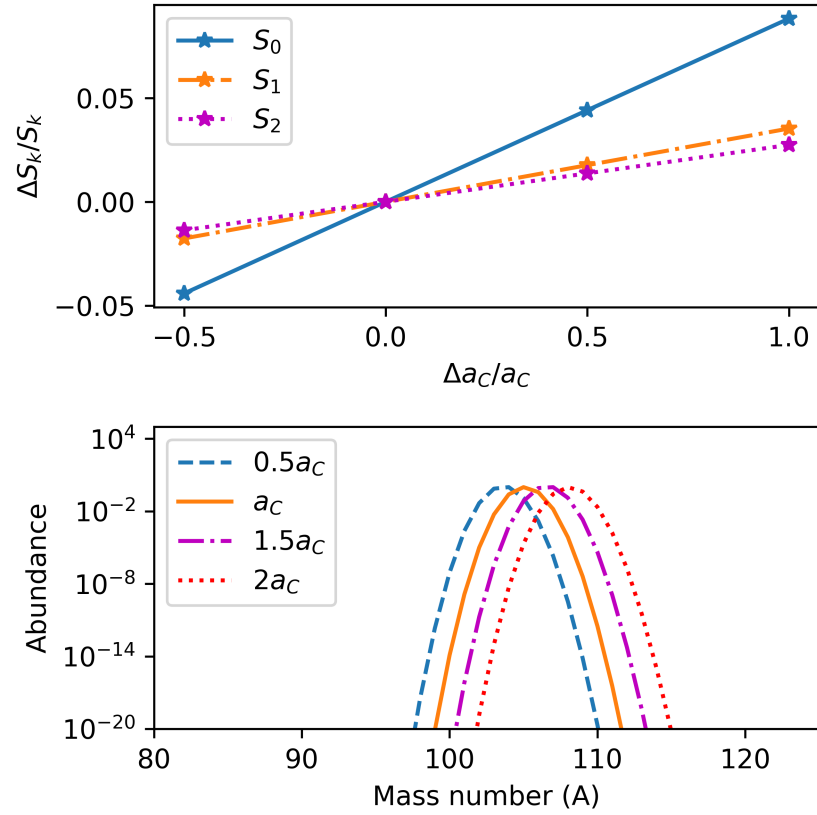


FIG. 18: (Color online) The same as Fig. 17 but for variation in the Coulomb term coefficient  $a_C$ .

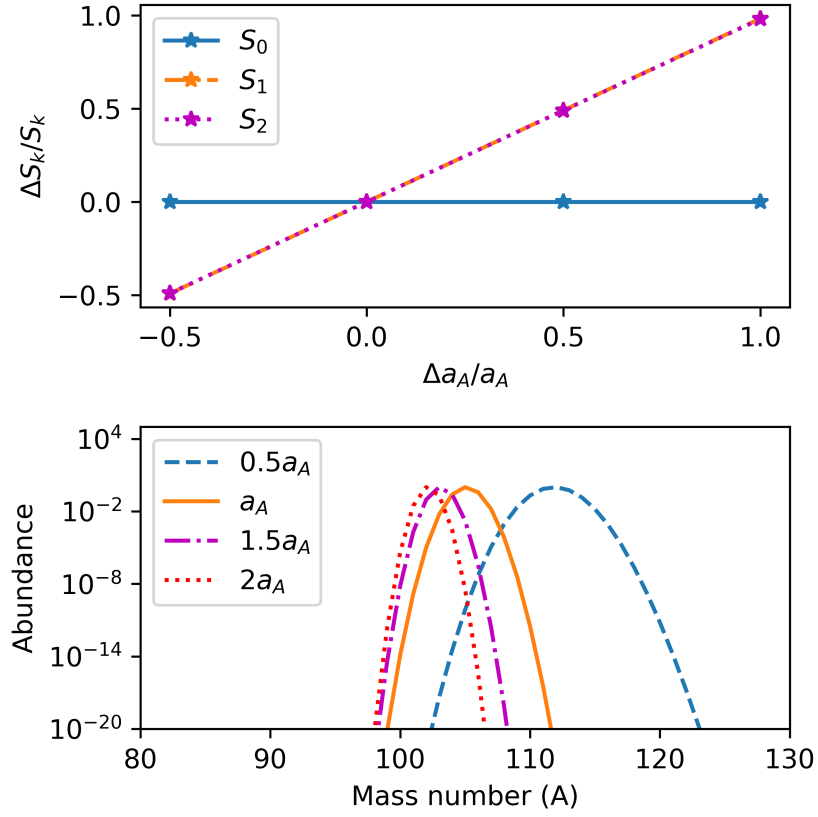


FIG. 19: (Color online) The same as Fig. 17 but for variation in the asymmetry term coefficient  $a_A$ .

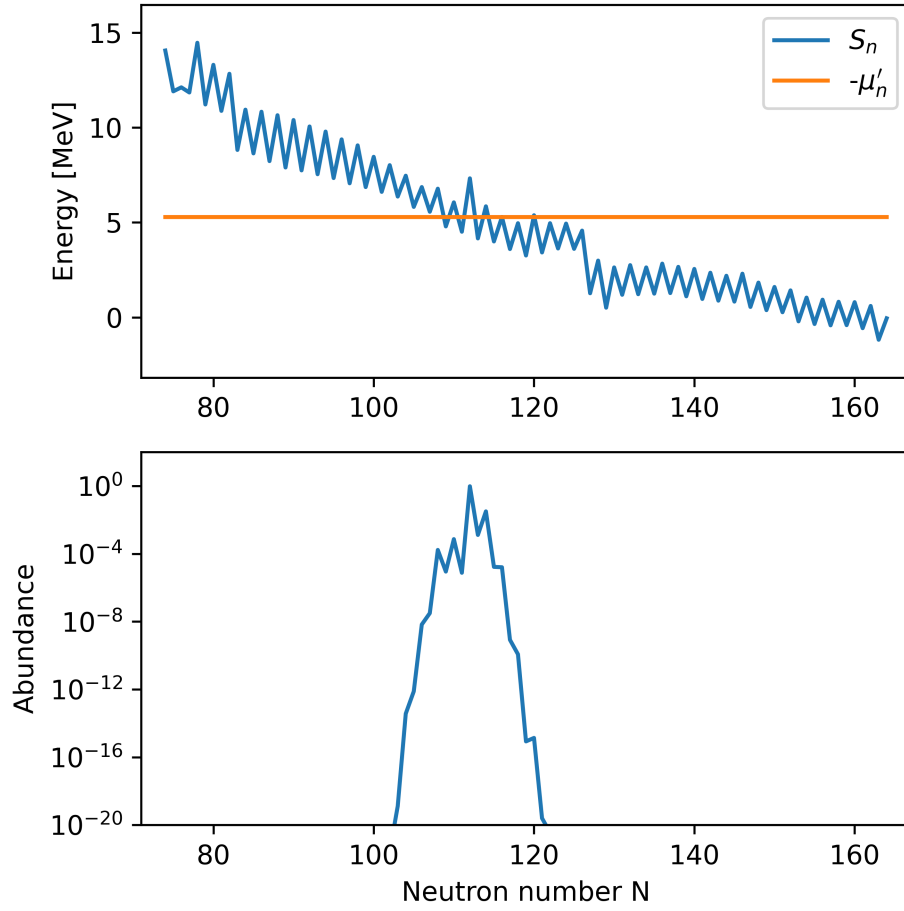


FIG. 20: (Color online) Results for  $Z = 70$ . The upper panel shows the intersection of  $S_n$  and the given  $-\mu'_n$ , and the lower panel presents the abundance distribution.

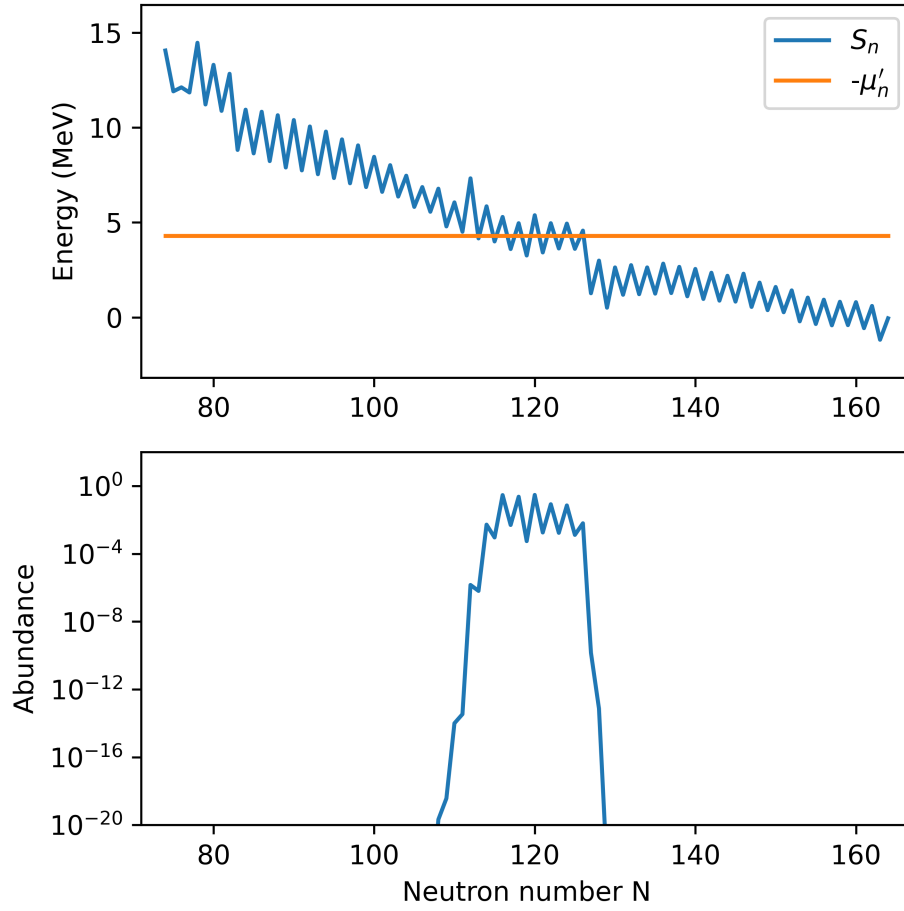


FIG. 21: (Color online) Results for  $Z = 70$ . The upper panel shows the intersection of  $S_n$  and the given  $-\mu'_n$ , and the lower panel presents the abundance distribution.

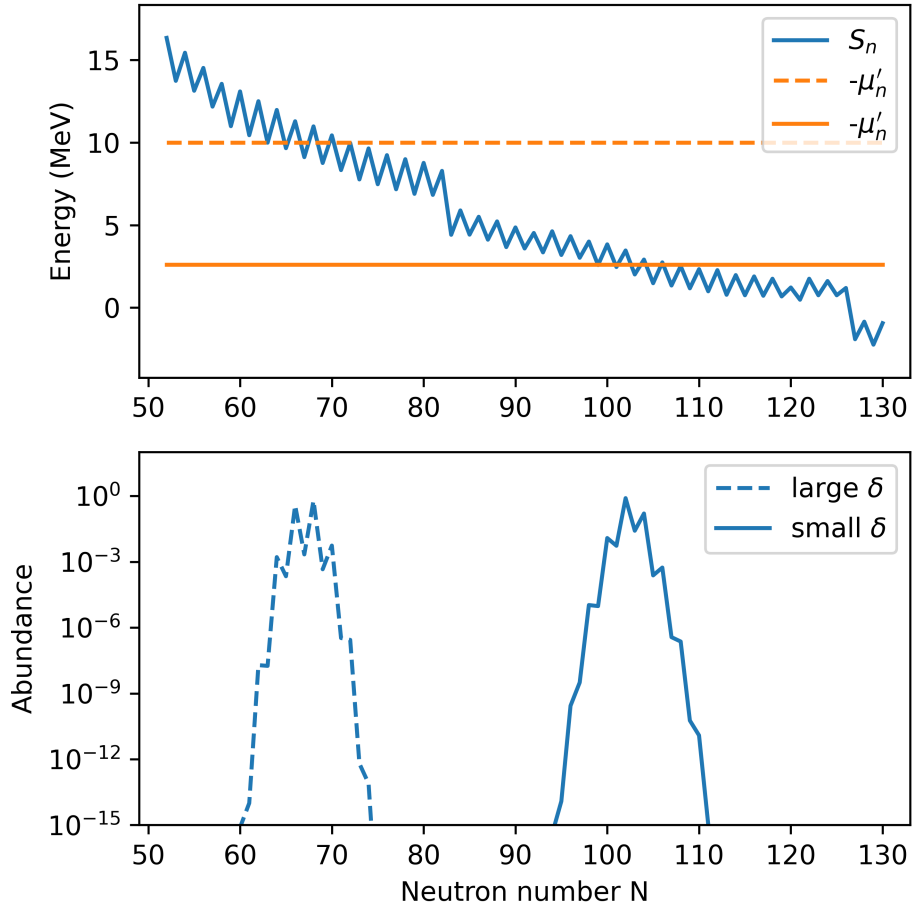


FIG. 22: (Color online) Results for  $Z = 55$ . The upper panel shows the intersections of energies. The lower panel presents the abundance distribution when the pairing effect in  $S_n$  is distinctive in each shell.

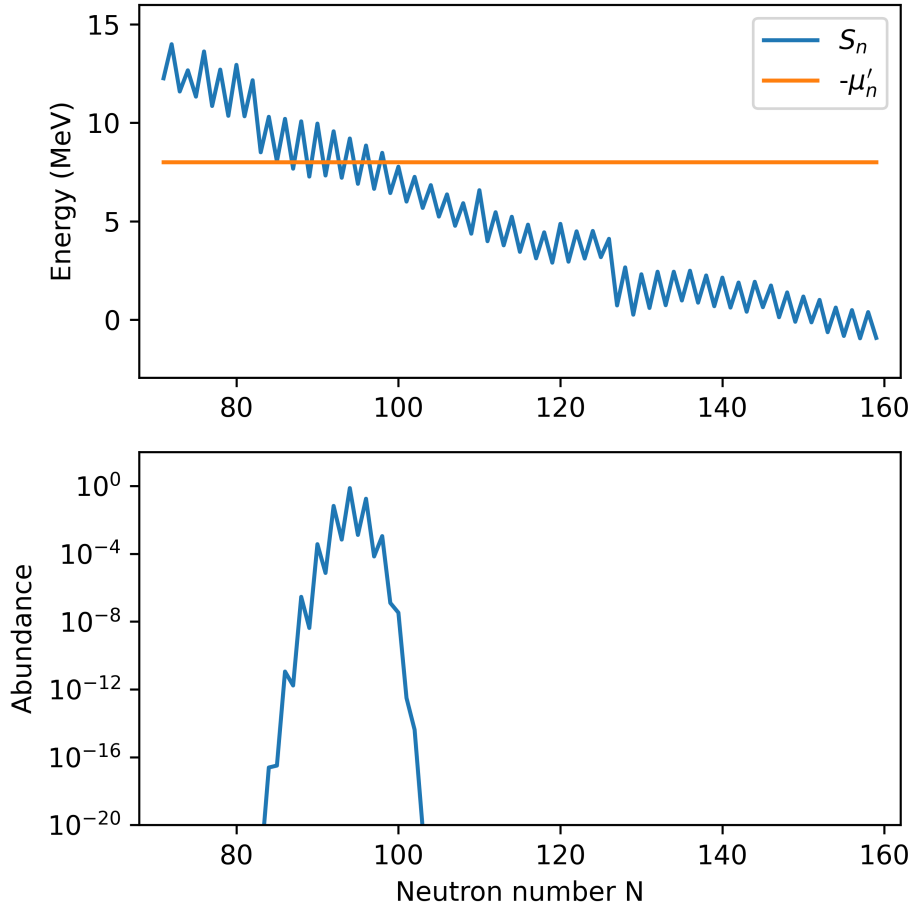


FIG. 23: (Color online) Results for  $Z = 68$ . The upper panel shows the intersections of energies. The lower panel demonstrates the abundance pattern when the pairing effect varies inside a single shell.

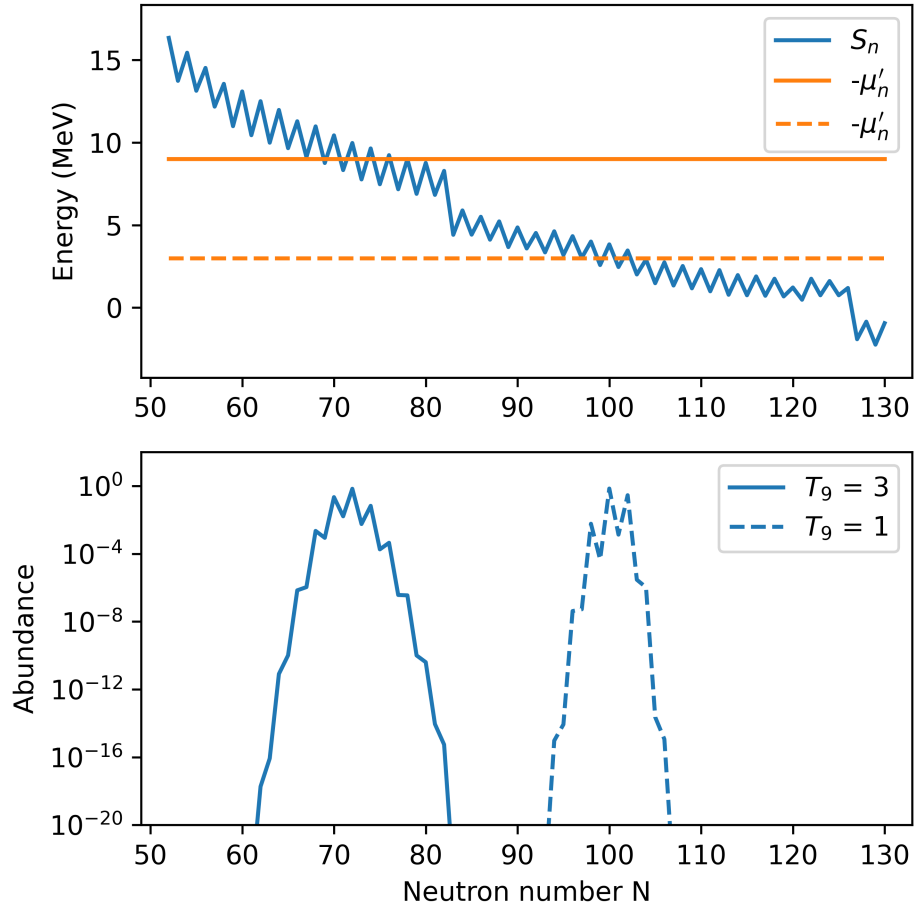


FIG. 24: (Color online) The upper panel shows the intersection of  $S_n$  and  $-\mu'_n$  (3 and 9 MeV). The lower panel presents the abundances distribution with different temperatures.

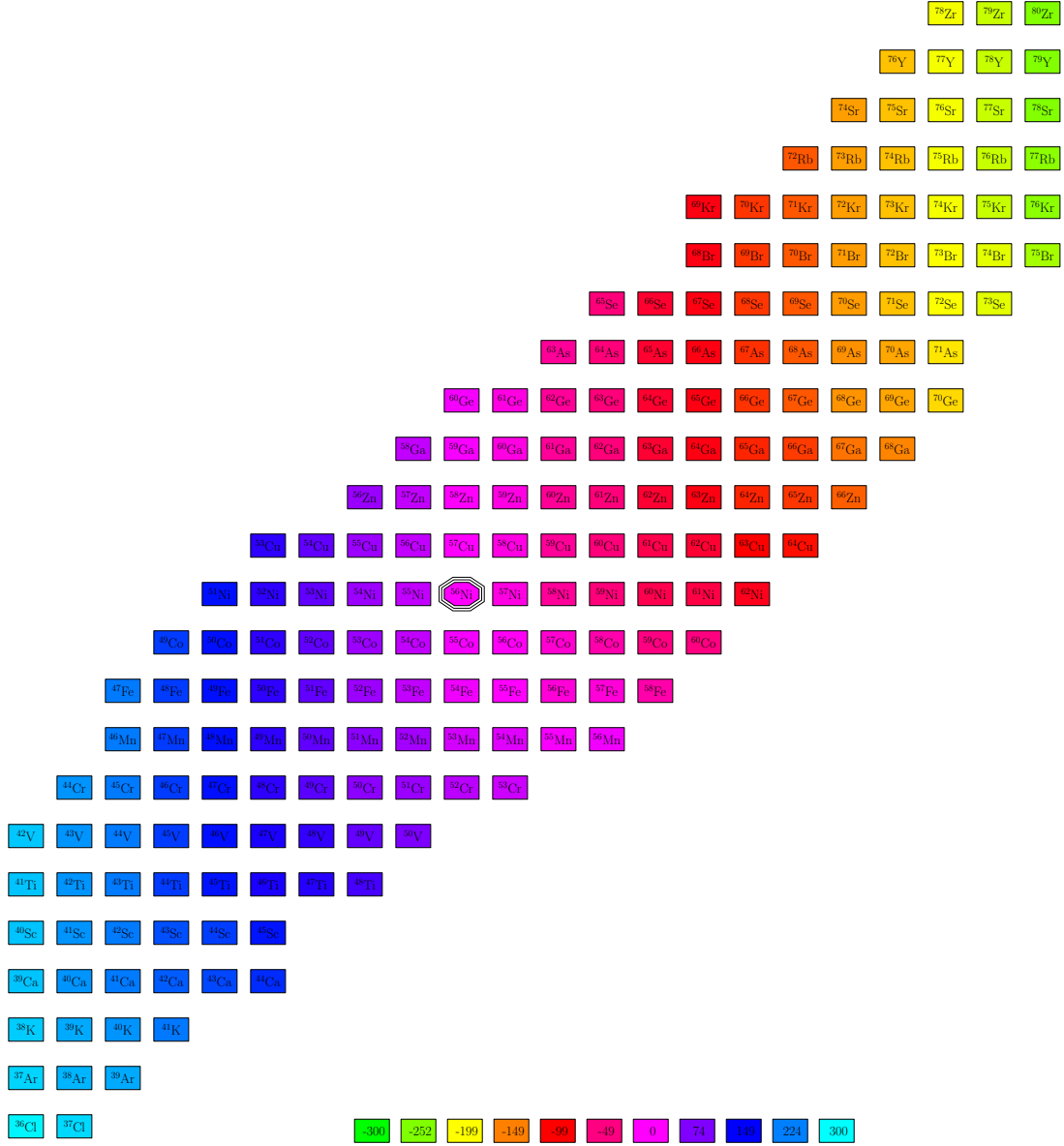


FIG. 25: (Color online) Chemical potential offset differences for the reference  $\nu p$ -process calculation at the time step  $t = 0.914$  s,  $T_9 = 2.18$ , and mass density  $\rho = 1.73 \times 10^5$  g/cc.

The color indicates the value chemical potential offset difference, and the value for any species may be inferred from the color bar.

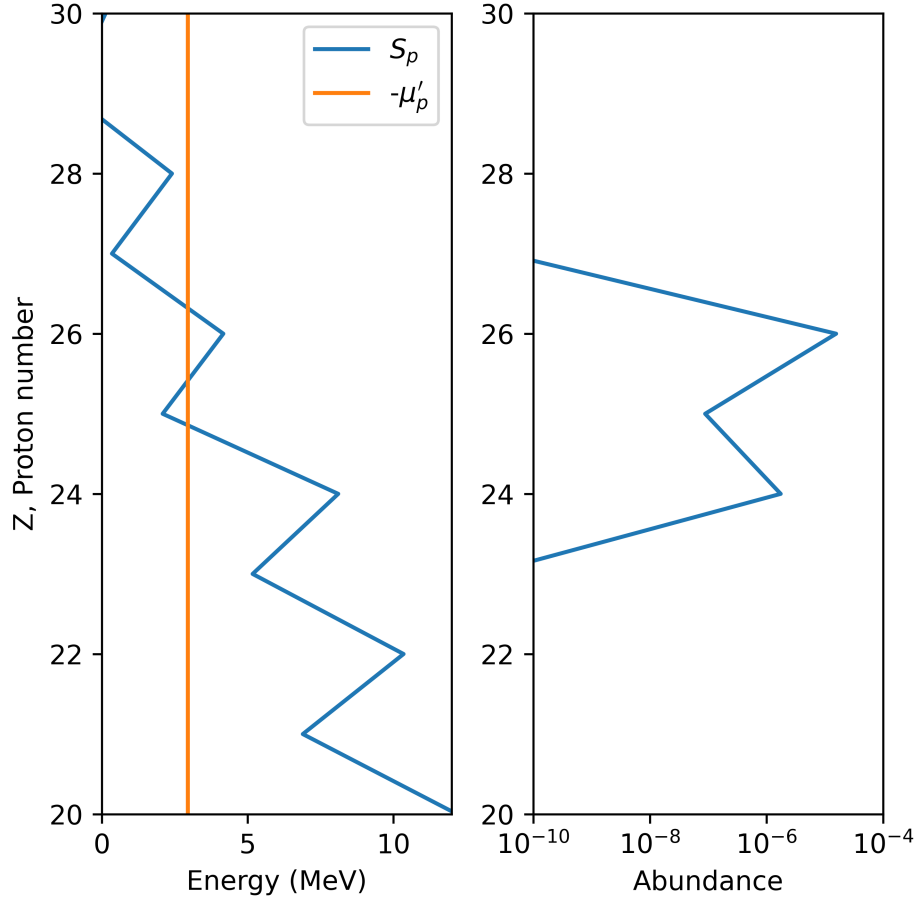


FIG. 26: (Color online) Relevant nuclear energies and abundances for the  $N = 24$  isotones in the  $\nu p$  process at the time step shown in Fig. 25. The left panel shows the intersection of proton-separation energy ( $S_p$ ) and proton chemical potential less proton rest mass energy ( $-\mu'_p$ ). The right panel presents the isotonic network abundances which overlap the  $(p, \gamma) - (\gamma, p)$  equilibrium abundances at this time step.